HHS Public Access

Author manuscript

Neuron. Author manuscript; available in PMC 2020 November 20.

Published in final edited form as:

Neuron. 2019 November 20; 104(4): 736–748.e6. doi:10.1016/j.neuron.2019.08.017.

Input-specific metaplasticity in the visual cortex requires Homer1a mediated mGluR5 signaling

Varun Chokshi[1,2], **Ming Gao**[1,3], **Bryce Grier**[1], **Ashley Owens**[1], **Hui Wang**[1,4], **Paul F. Worley**[5], **Hey-Kyoung Lee**[1,2,5,6,*]

[1]The Zanvyl Krieger Mind/Brain Institute, Johns Hopkins University, Baltimore, MD 21218, USA

[2]Cell Molecular Developmental Biology and Biophysics (CMDB) Graduate Program, Johns Hopkins University, Baltimore, MD 21218, USA

[3]Current address: Division of Neurology, Barrow Neurological Institute, Phoenix, AZ 85013, USA

[4]Current address: Epsilon, University of Cincinnati College of Business, Cincinnati, OH 45221, USA

[5]The Solomon H. Snyder Department of Neuroscience, Johns Hopkins School of Medicine, Baltimore, MD 21205, USA

[6]Kavli Neuroscience Discovery Institute, Johns Hopkins University, Baltimore, MD 21218, USA

Summary

Effective sensory processing depends on sensory experience-dependent metaplasticity, which allows homeostatic maintenance of neural network activity and preserves feature selectivity. Following a strong increase in sensory drive, plasticity mechanisms that decrease the strength of excitatory synapses are preferentially engaged to maintain stability in neural networks. Such adaptation has been demonstrated in various model systems including mouse primary visual cortex (V1), where excitatory synapses on layer 2/3 (L2/3) neurons undergo rapid reduction in strength when visually deprived mice are re-exposed to light. Here we report that this form of plasticity is specific to intracortical inputs to V1 L2/3 neurons, and depend on the activity of NMDA receptors (NMDARs) and Group I metabotropic glutamate receptor 5 (mGluR5). Furthermore, we found that expression of the immediate early gene (IEG) Homer1a (H1a) and its subsequent interaction with mGluR5s is necessary for this input-specific metaplasticity.

eTOC

*Corresponding Author and Lead Contact: Hey-Kyoung Lee, (tel.) 410-516-5712, heykyounglee@jhu.edu.

Author Contributions

Conceptualization, H.-K.L., V.C., P.F.W.; Methodology & Investigation, H.-K.L., V.C., M.G., B.G., A.O., H.W.; Formal Analysis, H.-K.L., V.C., M.G., B.G.; Resources, P.F.W.; Writing—Original Draft, H.-K.L., V.C.; Writing—Review & Editing, H.-K.L., V.C., B.G., P.F.W.; Visualization, V.C.; Supervision, H.-K.L., P.F.W.; Project Administration & Funding Acquisition, H.-K.L.

Declaration of Interests

PFW is a co-founder and serving as a Chief Scientific Officer of CogNext.

Chokshi et al. demonstrate that visual experience-induced expression of H1a and its interaction with mGluR5 selectively depresses intracortical synapses in an NMDAR-dependent manner. Such metaplasticity may benefit *in vivo* circuit function by allowing input-specific homeostatic control.

Graphical Abstract

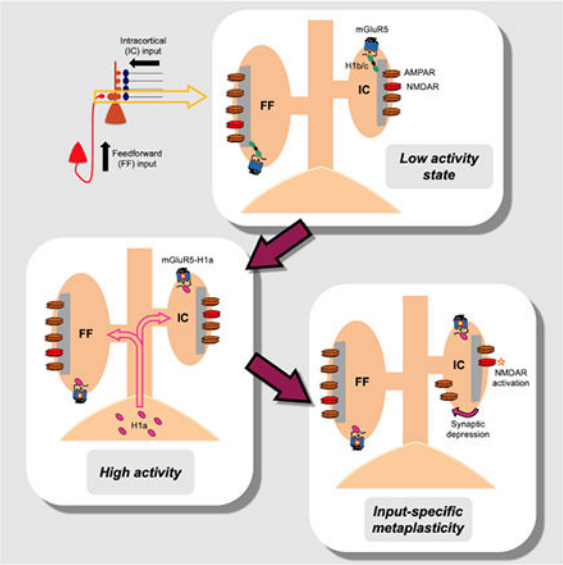

Keywords

visual cortex; metaplasticity; metabotropic glutamate receptor; mGluR5; H1a; NMDA receptor

Introduction

Visual experience guides the refinement of synaptic connections after the onset of vision. Mouse V1 has been widely used to study experience-dependent homeostatic plasticity mechanisms *in vivo* (Whitt et al., 2014). In juvenile mice, a few days of visual deprivation through dark exposure (DE) increases the strength of excitatory synapses onto V1 L2/3 pyramidal neurons, while restoring visual experience induces a rapid reduction of synaptic strength (Gao et al., 2010; Goel et al., 2006; Goel and Lee, 2007). Unlike Hebbian plasticity, which is triggered by rapid changes in input activity, changes in activity over longer timescales, such as with long-term alterations in visual experience, trigger homeostatic mechanisms to maintain network stability (Abbott and Nelson, 2000; Bear et al., 1987; Bienenstock et al., 1982; Cooper and Bear, 2012). There are largely two forms of homeostatic plasticity: sliding threshold metaplasticity and synaptic scaling. While the former slides the induction threshold for NMDAR-dependent plasticity (Bear et al., 1987; Bienenstock et al., 1982; Cooper and Bear, 2012), the latter is largely independent of NMDAR activity (Turrigiano, 2008; Turrigiano et al., 1998). Previous studies have shown that a few days of visual deprivation upregulates synaptic expression of GluN2B containing NMDARs, which promotes LTP in L2/3 of V1 (Guo et al., 2012; Philpot et al., 2003; Philpot et al., 2001; Quinlan et al., 1999). Recently, it was demonstrated that visual deprivation-

induced upregulation of miniature excitatory postsynaptic currents (mEPSCs) in L2/3 of V1 is dependent on GluN2B and elevated spontaneous activity (Bridi et al., 2018). These results support the idea that visual deprivation-induced strengthening of excitatory synapses in V1 L2/3 is due to sliding threshold model of metaplasticity, in which elevated spontaneous activity acts on GluN2B containing NMDARs to promote potentiation across a large number of synapses. We recently reported that mEPSCs generally reflect the strength of lateral intracortical (IC) inputs to V1 L2/3 neurons, but do not capture changes occurring at sparse inputs such as feedforward (FF) synapses from L4 (Petrus et al., 2015). We found that IC inputs onto V1 L2/3 neurons become stronger in response to DE, while the strength of FF synapses from L4 remains constant. These results suggest that in intact circuitry where different inputs receive different patterns of activity, homeostatic synaptic adjustment occurs in an input-specific manner. To date, Arc and retinoic acid have been shown to play roles in input-specific strengthening of synapses by inactivity (Beique et al., 2011; Yee et al., 2017). It is currently unknown whether input-specific homeostatic plasticity occurs when there is an abrupt increase in input activity, and if so, what the molecular mechanisms mediating this phenomenon are.

When visual deprivation is reversed by re-exposure to light, the average size of mEPSCs in V1 L2/3 neurons is reduced (Gao et al., 2010; Goel et al., 2006; Goel and Lee, 2007). Here we report that this change is restricted to the lateral IC inputs and is not present at the FF synapses from L4. Furthermore, input-specific downregulation of IC synapses requires activity of NMDARs and mGluR5s, both of which have been implicated in metaplasticity (Abraham, 2008; Cohen and Abraham, 1996). Mechanistically, we found that the immediate early gene H1a and its interaction with mGluR5 are necessary for this input-specific metaplasticity.

Results

Weakening of excitatory synapses with visual experience requires agonist-independent activity of mGluR5

Given that mGluRs are localized at perisynaptic loci, we reasoned that they may detect glutamate spillover during abrupt increases in synaptic activity, as would occur when DE mice are brought out to light. To test whether mGluR activity is required for weakening synapses with light re-exposure, we first used pharmacological inhibitors of Group I mGluRs to allow acute manipulations of specific subtypes. Synaptic strength was assessed by measuring mEPSCs recorded from pyramidal neurons in L2/3 of V1 from normal reared (NR), 2 days DE, and DE mice that received 2 hours of subsequent light exposure (LE) in the presence or absence of specific mGluR antagonists (Figure 1A).

We first tested the involvement of mGluR5, expressed on postsynaptic spines (Lopez-Bendito et al., 2002), by blocking both agonist-dependent and agonist-independent activity (Pagano et al., 2000) with an inverse agonist, 2-methyl-6-(phenylethynyl) pyridine hydrochloride (MPEP, 10 mg/kg i.p. once daily) (Tsanov and Manahan-Vaughan, 2009). The control group (PBS, i.p. once daily) exhibited normal bidirectional changes in synaptic strength as previously found (Goel and Lee, 2007): the average mEPSC amplitude was increased by DE and reverted to normal levels by subsequent LE (Figure 1B). NR mice that

received MPEP (2 days) had higher basal synaptic strength than the controls (Figure 1B,C; t-test, p=0.01), which was multiplicative (Figure 1D). This suggests that mGluR5 activity maintains a lower basal synaptic strength during normal visual experience. We did not observe further increase in mEPSC amplitude in mice treated with MPEP during DE, which suggests occlusion of DE induced synaptic strengthening. More importantly, when DE mice received MPEP injection immediately before light re-exposure (i.p. 30 min before LE), mEPSC amplitudes did not decrease following LE (Figure 1C). Again, mEPSC frequency was similar across groups (Figure 1 E,F). These data indicate that mGluR5 activity is required for experience-dependent reduction in excitatory synaptic strength during normal visual experience and LE condition in V1 L2/3.

Next, we tested whether the effect was specific to mGluR5 among Group1 mGluRs. In contrast to MPEP, mGluR1 inhibition by AIDA (1 mg/kg, i.p. once daily for 2 days), a competitive antagonist of mGluR1, did not affect basal amplitude of mEPSCs, but blocked increases with DE (Figure S1A–C). AIDA treatment to DE mice immediately prior to LE did not block the decrease in mEPSC amplitudes (Figure S1B). While the average mEPSC amplitudes of PBS and AIDA treated NR groups were not statistical different, there was multiplicative reduction in mEPSC amplitudes in the AIDA group (Figure S1C). There was no significant changes in mEPSC frequency across groups (Figure S1D). We rule out the possibility that the differential effect of AIDA and MPEP is due to the ability of MPEP to block both agonist-dependent and independent activity while AIDA only blocks the former, by replicating the AIDA results using an inverse agonist of mGluR1, Bay36-7620 (20 mg/kg i.p. once daily) (Gil-Sanz et al., 2008) (Figure S1E–H). These results suggest that mGluR1 plays a distinct role from mGluR5 in that it supports strengthening of synapses with visual deprivation. Collectively, our results suggest that mGluR5 activity is specifically required for weakening excitatory synapses with visual experience.

Visual experience specifically weakens lateral IC inputs to L2/3 neurons

V1 L2/3 neurons receive strong FF inputs from L4 principal neurons, but these constitute a small portion of the total inputs (Binzegger et al., 2004; Douglas and Martin, 2004). The rest of the inputs are IC connections from local L2/3 neurons, deeper V1 layers, higher order visual areas, and other cortical areas (Dantzker and Callaway, 2000; Iurilli et al., 2012; Schroeder and Foxe, 2005; Xu et al., 2016; Yang et al., 2013). Previously, we reported that DE only potentiates IC inputs without changes in FF inputs in V1 L2/3 neurons (Petrus et al., 2015). These findings also suggested that mEPSCs mainly represent IC inputs, and that homeostatic synaptic plasticity driven by visual deprivation is input-specific.

We determined whether homeostatic plasticity induced by increased visual experience is also input-specific. We measured the strength of individual synapses in an input-specific manner by recording Sr^{2+} desynchronized evoked EPSCs from V1 L2/3 neurons. To specifically activate FF inputs from L4 to L2/3, we injected an adeno-associated virus containing double-floxed channelrhodopsin-2 (AAV9.EF1.dflox.hChR2(H134R)-mCherry or AAV9.EF1a.DIO.hChR2(H134R).EYFP) into V1 of Scnn1a-Tg3-cre (L4-Cre) mice (see STAR methods). IC inputs to V1 L2/3 neurons were stimulated by an electrode placed in L2/3 lateral to the recorded neuron (Figure 2A). In the presence of Sr^{2+}, evoked responses

result in desynchronized release of vesicles (Abdul-Ghani et al., 1996; Dodge et al., 1969; Gil et al., 1999; Oliet et al., 1996). These desynchronized single vesicle events are considered mEPSCs (Sr^{2+}-mEPSCs) resulting from the stimulated input, and can be analyzed to measure the strength of individual synapses participating in evoked synaptic transmission (Figure 2B). We calculated the average amplitude of evoked Sr^{2+}-mEPSCs by subtracting out the contribution of spontaneous mEPSCs (see STAR Methods for detail).

IC inputs potentiated with DE and reverted back to normal levels with a subsequent LE (Figure 2C), which mirrored mEPSC changes. However, the strength of FF inputs from L4 did not alter significantly (Figure 2D). This indicates that visual experience drives homeostatic plasticity in an input-specific manner in L2/3 neurons through selective weakening of IC inputs. Mechanistically, the specific weakening of IC inputs with visual experience was dependent on NMDAR and mGluR5 activity. This was demonstrated by administering either the NMDAR antagonist CPP (10 mg/kg, i.p.) or the mGluR5 inverse agonist MPEP (10 mg/kg, i.p.) to DE mice 30 min prior to LE. In CPP or MPEP injected mice, IC inputs failed to depress in response to LE (Figure 2E) without effect on FF evoked Sr^{2+}-mEPSC amplitudes (Figure 2F). Our results indicate a novel dual requirement of NMDAR and mGluR5 activity for input-specific depression of IC synapses with LE.

H1a is required for visual experience-dependent weakening of excitatory inputs

Homer1 proteins regulate agonist-independent activity of Group I mGluRs (Ango et al., 2001; Tu et al., 1998) and the coupling of mGluRs to downstream signaling pathways (Kammermeier and Worley, 2007; Kammermeier et al., 2000; Park et al., 2013). The long forms of Homer1 (H1b/c and H3) block constitutive activity of mGluRs (Ango et al., 2001) and restrict receptors to small clusters within synaptic sites (Ango et al., 2000; Kammermeier et al., 2000). However, when the activity-dependent variant of Homer1 (H1a) is expressed, Group I mGluRs disperse across the dendrites and become constitutively active. Both H1a and long forms of Homer1 share the EVH1 domain, which binds to its effectors including Group 1 mGluRs (Tu et al., 1999; Tu et al., 1998). In dissociated neuronal cultures, H1a mediates homeostatic downscaling induced by pharmacologically increasing activity (Hu et al., 2010). This action of H1a that activates agonist-independent mGluR5 signaling is upstream of Arc (Hu et al., 2010), which is also required for downscaling excitatory synapses in V1 (Gao et al., 2010). Furthermore, it was shown that visual experience following dark-rearing rapidly induces H1a mRNA expression in V1 (Brakeman et al., 1997).

Based on our result that mEPSC amplitude measurement reflects the strength of IC inputs, we examined the involvement of H1a in the experience-dependent synaptic weakening by recording mEPSCs in V1 L2/3 neurons in H1a knockout mice (H1aKO) (Hu et al., 2010). We confirmed that there was no expression of H1a in V1 of these animals (Figure S2A) albeit an increase in H1b/c mRNA and protein levels (Figure S2B,C).

We found that genetic KO of H1a affected mEPSCs in a manner similar to that of pharmacological inhibition of mGluR5 in wildtype mice. This is consistent with the notion that H1a triggers mGluR5 agonist-independent signaling (Ango et al., 2001). Basally, H1aKOs showed elevated mEPSC amplitudes compared to H1aWTs (t test, $p<0.01$), which

was multiplicative suggesting that most of the sampled synapses undergo change (Figure 3A–D). The abnormal enhancement of basal mEPSC amplitude seen in H1aKOs was not likely due to gross changes in the expression of glutamate receptors, because we did not find significant changes in either the surface or total levels of several glutamate receptor subunits in microdissected V1 L2/3 slices processed for surface biotinylation (Figure S3A). In H1aKOs, the effect of DE was occluded by the increased basal synaptic strength, and more importantly these mice lacked LE induced decrease in mEPSC amplitudes (Figure 3C). These findings contrast the normal bidirectional regulation observed in H1aWTs (Figure 3B). There was no significant change in mEPSC frequency across groups (Figure 3E). Our results suggest that H1a is required for experience-dependent weakening of synapses in V1 L2/3 neurons during NR and LE conditions.

H1aKO animals display normal early developmental change in mEPSCs

mEPSCs in V1 L2/3 neurons decrease in amplitude and increase in frequency around P14, which coincides with eye-opening in mice (Goel and Lee, 2007). We tested whether the high basal mEPSC amplitude of H1aKOs reflects a failure of this developmental process. We compared the mEPSCs of NR mice before eye opening (P11-P12) and during the critical period (P23-P32) (Figure 4A). H1aKOs displayed comparable mEPSC amplitudes at P11-P12 to H1aWTs (Figure 4B,C). Like H1aWTs, H1aKOs also exhibited a developmental decrease in mEPSC amplitudes, but the average amplitude did not decrease to the same level (Figure 4B,C). In parallel, H1aKOs showed a normal developmental increase in mEPSC frequency (Figure 4D). Thus, H1aKOs seem to undergo largely normal early development of excitatory synaptic transmission in V1 L2/3 neurons upon eye-opening. Our results also highlight that there are two distinct mechanisms for the developmental decrease in mEPSC amplitude: a major component that is independent of H1a and a minor component that is dependent on H1a, as seen by the small but significantly elevated mEPSC amplitude in 3 weeks old H1aKOs (also see Fig. 3D).

To address the role of mGluR5 signaling in these developmental processes, we performed daily MPEP injections (10 mg/kg, i.p. once daily) starting at P14, when mice typically open their eyes. mEPSC recordings were done at P23-32. MPEP treated mice showed significantly larger mEPSC amplitude (Fig. 4C), but also higher mEPSC frequency (Fig. 4D). Elevated mEPSC frequency is reminiscent of that observed in L4 neurons in barrel cortex of mGluR5KO (Ballester-Rosado et al., 2010), which suggests that mGluR5 may have an effect on mEPSC frequency which is not likely through H1a. Collectively, these results suggest that mGluR5 and H1a play a relatively minor role in establishing normal excitatory synaptic strength during postnatal development.

Postnatal H1a expression in V1 is required for experience-dependent weakening of excitatory synapses

Given that our H1aKO is global and constitutive, we wanted to rule out any adverse effect resulting from globally lacking H1a during early development. To attain temporal and spatial control of H1a expression, we employed mice harboring a Cre-inducible conditional knockout of the Homer1 gene ($Homer1^{fl/fl}$) (Figure 5A). This conditional KO is not specific for H1a, however, and also affects the constitutively expressed long forms of Homer1

(H1b/c). To have specific temporal and spatial control over H1a, we crossed mice expressing the conditional KO of Homer1 to H1aKO mice to generate H1b/$c^{fl/+}$;$H1a^{fl/-}$ mice. By targeting viral mediated CaMKII promoter-driven Cre expression postnatally (P21-30) to V1, we generated V1 neurons with three different genotypes as delineated in Figure 5A: H1b/$c^{+/+}$;$H1a^{+/-}$, H1b/$c^{+/-}$;$H1a^{-/-}$ and H1b/$c^{+/-}$;$H1a^{+/-}$. Transfected cells were identified for recording by GFP expression driven by the viral construct. mEPSCs recorded in L2/3 neurons with conditional H1aKO (H1b/$c^{+/-}$;$H1a^{-/-}$) were similar to those seen in constitutive H1aKOs: The basal mEPSC amplitude was higher than in cells recorded from the other two lines in which V1 neurons were heterozygous for H1a (Figure 5B–D). More importantly, conditional H1aKO (H1b/$c^{+/-}$;$H1a^{-/-}$) neurons did not exhibit experience-dependent synaptic weakening with LE (Figure 5C). It is important to note that conditional H1aKO neurons are heterozygous for H1b/c. Neurons heterozygous for H1a only (H1b/$c^{+/+}$;$H1a^{+/-}$) or for both splice variants of Homer1 (H1b/$c^{+/-}$;$H1a^{+/-}$) displayed normal experience-dependent plasticity (Figure 5B,D). Thus, H1a is haplo-sufficient to support this form of plasticity. The frequency of mEPSCs did not change significantly across groups (Figure 5B–D). To ensure that the KO of H1a was successful in the conditional knockouts (H1b/$c^{+/-}$;$H1a^{-/-}$), we performed quantitative PCR and found significantly reduced H1a and H1b/c mRNA levels compared to control H1b/$c^{+/+}$;$H1a^{+/-}$ mice (Figure S4A,B). We also confirmed that GFP expression was comparable in two of the groups that received viral transfections (Figure S4C). Our data indicate that postnatal H1a expression in V1 is required for weakening excitatory synapses with visual experience.

Interaction between mGluR5s and Homer is required for experience-dependent weakening of V1 L2/3 synapses

The preceding experiments suggest that agonist-independent mGluR5 activity and H1a are critical for depressing mEPSCs upon visual experience. However, mGluR5s are not the only targets of H1a (Kato, 2009; Shiraishi-Yamaguchi and Furuichi, 2007; Tu et al., 1999; Tu et al., 1998). To test the specific role of H1a and mGluR5 interaction, we examined two different knockin (KI) mice with mutations that target the Homer binding site on mGluR5s (1123TPPSPF) and reduce the binding affinity of Homer1 EVH1 domain. The first line contains the substitutions T1123A and S1126A on mGluR5s (TSKI), which reduce EVH1 binding affinity by 4~10 times (Park et al., 2013). In the TSKIs, the basal synaptic strength was significantly higher than in TSWTs (Figure 6A,B; t test, $p<0.005$), and this difference was multiplicative (Figure 6C). Similar to H1aKOs, this increase in basal synaptic strength occluded the potentiation of synapses by DE. Importantly, TSKIs also lacked depression of synapses following LE, mirroring the effect seen in H1aKOs. There was no significant difference in mEPSC frequency across groups (Figure 6D). TSKIs expressed comparable levels of glutamate receptors in L2/3 of V1, except for a significantly higher surface expression of the NR2A subunit (Figure S3C).

The second line contained the F1128R mutation on mGluR5s (FRKI), which reduces the affinity of Homer1 EVH1 binding by ~50 folds (Park et al., 2013). FRKIs specifically lack H1a interaction without impact on mGluR5 signaling through a prolyl isomerase Pin1 (Park et al., 2013), which is not the case for TSKIs or H1aKOs. Despite this difference, FRKIs showed an elevated basal mEPSC amplitude compared to FRWTs (Figure 6E,F; t test,

p<0.05), but unlike that seen in H1aKOs (Figure 3D) or in TSKIs (Figure 6C), the increase was not multiplicative (Figure 6G). Nevertheless, FRKIs exhibited neither DE induced potentiation nor LE induced weakening of synapses (Figure 6F), similar to H1aKOs and TSKIs. There was no significant difference in the average mEPSC frequency across groups (Figure 6H). Results from TSKIs and FRKIs provide evidence for a role of mGluR5 and Homer1 interaction in mediating experience-dependent weakening of synapses during normal vision and LE.

Input-specific regulation of IC inputs is mediated by mGluR5-H1a signaling

While measurements of mEPSCs mainly reflect IC inputs (Figure 1 and 2), we wanted to confirm that mGluR5 signaling through H1a acts in an input-specific manner. To do this, we crossed L4-Cre and FRKI mice to generate L4Cre;FRKI mice, which allowed us to drive ChR2 expression in L4 neurons in the FRKI genotype. The rationale for choosing FRKIs was that, unlike H1aKOs or TSKIs, they have preserved mGluR5 signaling through Pin1, which has been implicated in potentiating NMDAR responses (Park et al., 2013). Therefore, the use of FRKIs avoids any potential confounds of altering Pin1 signaling. In L4Cre;FRKIs, we found that experience-dependent plasticity of IC inputs is abolished (Figure 7A). This suggests that H1a-induced agonist-independent signaling of mGluR5 is critical for mediating input-specific metaplasticity. Unexpectedly, we also observed an aberrant strengthening of FF inputs with LE in L4Cre;FRKIs (Figure 7B). One possibility may be due to unmasking of synaptic potentiation in the absence of mGluR5-H1a dependent metaplasticity. According to the sliding threshold model, enhanced activity with LE would increase the threshold for LTP. Hence, blocking mGluR5-H1a dependent metaplasticity would prevent the change in synaptic modification threshold and promote potentiation of inputs that normally would be subthreshold for inducing LTP. Consistent with this idea, we found that injection of NMDAR antagonist CPP (10 mg/kg, i.p.) 30 min prior to LE prevented the aberrant potentiation of FF inputs in L4Cre;FRKIs without affecting IC inputs (Fig. 7C,D). In conclusion, we demonstrated that restoring visual experience triggers input-specific weakening of IC synapses, which is dependent on NMDAR activity and mGluR5 signaling through interaction with H1a. Collectively, our results support the metaplasticity model of homeostatic adaptation, which could explain the input-specific nature of synaptic changes.

Discussion

We found that an increase in visual experience induces input-specific depression of IC synapses onto V1 L2/3 pyramidal neurons without affecting FF synapses from L4 (Figure 2C,D). Changes in mEPSC amplitudes mainly reflect the more abundant IC inputs (Figures 1A,2C&D,3A). Visual experience-induced input-specific synaptic depression was dependent on NMDARs (Fig. 2E), which suggests the involvement of the sliding threshold model of metaplasticity. In addition, this form of metaplasticity was dependent the agonist-independent activity of mGluR5 triggered by its interaction with H1a (Figures 1,2,3,5,6,7).

Agonist-independent activity of specific Group I mGluR subtypes mediate opposing metaplasticity

Acute pharmacological inhibition of individual Group I mGluRs revealed that specific subtypes of mGluRs play distinct functions in bidirectional regulation of excitatory synapses. Inhibiting the agonist-independent activity of mGluR5s, using a specific inverse agonist, blocked visual experience-dependent synaptic depression (Figure 1), while an inverse agonist of mGluR1 prevented DE-mediated synaptic potentiation (Figure S1). There is precedence for differential roles of these two types of mGluRs in a traumatic brain injury model, where mGluR1 activity increases cell death and mGluR5 activation is required for neuroprotection (Luo et al., 2014).

Future experiments are needed clarify the role of agonist-independent mGluR1 signaling mechanisms that support the synaptic potentiation (Figure S1). Recent work in V1 (Bridi et al., 2018) suggested that DE-mediated potentiation of mEPSCs may require molecular mechanisms capable of sensing small increases in spontaneous firing. A recent imaging study using an optical glutamate sensor estimated that extrasynaptic glutamate concentration increases to micromolar levels with neural activity (Okubo et al., 2010). The affinity of Group1 mGluRs to glutamate is well within the range to sense such small changes (Conn and Pin, 1997). Furthermore, DE increases the rate of spontaneous burst firing (Bridi et al., 2018), which would be conducive for the glutamate spillover needed to activate perisynaptic mGluRs. While it is currently unclear how mGluR1 and mGluR5 respond differentially to neural activity accompanying changes in visual experience, there are differences in downstream signal coupling that may lead to opposite outcome on synaptic plasticity. The downstream Ca^{2+} increase resulting from mGluR1 activation occurs as a single transient burst, whereas mGluR5 signaling drives Ca^{2+} oscillations (Kim et al., 2005). A transient large increase in intracellular Ca^{2+} is sufficient to potentiate synapses, while prolonged Ca^{2+} signals tend to depress synapses (Yang et al., 1999). Hence such differences in the time course of Ca^{2+} transients may lead to opposing synaptic changes. It is of importance to note that both the potentiation of mEPSCs with DE (Bridi et al., 2018) and depression of mEPSCs with LE are dependent on NMDARs (personal communication, G. Rodriguez and H-K Lee), which supports the interpretation that these homeostatic changes are due to the sliding threshold model of metaplasticity.

H1a acts as a visual experience sensor to depress IC inputs

We found that mGluR5 and its interaction with H1a is necessary for input-specific metaplasticity (Figure 2, 7). H1a expression is induced in cultured neurons by high activity upon blocking inhibition (Hu et al., 2010), and *in vivo* in various models designed to elevate activity such as increased visual activity (Brakeman et al., 1997), artificially generated seizures (Cavarsan et al., 2015; Cavarsan et al., 2012; Hu et al., 2010), traumatic brain injury (Luo et al., 2014), and pain desensitization (Tappe et al., 2006). Activity-dependent expression of H1a has also been proposed to play a neuroprotective role in NMDAR-induced neuronal injury (Wang et al., 2015), potentially through decoupling Ca^{2+} signaling pathways between NMDARs and mGluR5.

By using several genetic models, we have demonstrated that H1a is required for mGluR5-mediated input-specific metaplasticity triggered by an increase in visual activity. Specifically, mGluR5 and H1a interaction is necessary, as demonstrated by the lack of homeostatic adaptation in mice carrying mutations of mGluR5 that reduce its interaction with Homer1. It was shown in cell culture experiments that H1a mediated interruption of mGluR5-Homer1 crosslinking mediates a shift in mGluR5 signaling to an agonist-independent form (Ango et al., 2001). Additionally, in mouse models with enhanced association of mGluR5 and H1a produces greater mGluR5-dependent LTD (Ronesi et al., 2012).

Previous studies in culture neurons have implicated H1a in global synaptic scaling induced by pharmacological manipulations of neural activity (Hu et al., 2010). This global scaling could be a property of dissociated neuronal cultures, as the synaptic inputs are likely uniform in that model system. In contrast, V1 L2/3 neurons receive diverse sets of inputs arising from different areas including other sensory cortices in addition to FF inputs from L4 (Iurilli et al., 2012; Schroeder and Foxe, 2005; Thomson and Lamy, 2007). Therefore, changes in visual experience are expected to affect the activity of distinct inputs differently, thus requiring input-specific homeostatic adaptation as we report here (Figure 2). The selective depression of IC inputs with LE and our previous work showing specific potentiation of IC inputs with DE (Petrus et al., 2015) suggests that IC synapses may be more plastic for bidirectional homeostatic control. A recent study demonstrated plasticity of excitation to inhibition (E/I) balance in local recurrent inputs to L4 of V1, but not FF thalamocortical inputs, following monocular deprivation (Miska et al., 2018), which further suggests sensory manipulations can lead to input specific changes in synaptic function. Our results are also consistent with an emerging idea that input-specific mechanisms, like metaplasticity, are more relevant for homeostatic regulation of intact circuits *in vivo* (Bridi et al., 2018). Furthermore, it was suggested that input-specific homeostatic adaptation allows better information processing capacity of neural networks (Barnes et al., 2017), hence it is expected to benefit cortical function.

Concerted action of mGluR5 and NMDAR in mediating input-specific metaplasticity

mGluR5s have been implicated in metaplasticity. Specifically, they can prime synapses for induction of NMDAR-dependent LTP (Abraham, 2008; Bortolotto et al., 1994; Cohen and Abraham, 1996), and also increase the threshold for LTP (Matta et al., 2011). Given their perisynaptic location (Lopez-Bendito et al., 2002), mGluR5s are well-poised to detect glutamate spillover with high synaptic activity. Since LE-induced depression is input-specific and depends on NMDAR activity (Figure 2E), we propose that H1a induced agonist-independent mGluR5 signaling mediates the increase in the threshold for the induction LTP. H1a is specifically targeted to spines via input specific activation of NMDARs and downstream activation of PKG (Okada et al., 2009). Thus, H1a could increase the synaptic modification threshold is via direct inhibition of NMDAR function by mGluR5. It was demonstrated that mGluR5s are held away from NMDARs by its interaction with Homer1 and Shank scaffolds (Moutin et al., 2012). However, upon H1a expression, mGluR5s become detached from their synaptic scaffold and directly bind and inhibit NMDARs (Moutin et al., 2012). Such inhibition is predicted to increase the synaptic

modification threshold to promote synaptic depression as observed in our study. Another aspect of mGluR5 signaling would also explain the input-specific nature of such metaplasticity. mGluR5 is phosphorylated at the Homer EVH1 binding site by proline-directed kinases that can be activated by PKG, which creates a binding site for Pin1 (Park et al., 2013). mGluR5-Pin1 signaling is dependent on H1a, potentiates NMDAR currents and prevents depotentiation (Park et al., 2013). Accordingly, this pathway may create the synaptic tag for input specificity and bidirectional control of synaptic strength (Marton et al., 2015). Hence, based on the specific complement of intracellular signals triggered at individual synapses, even with global increases in H1a expression certain synapses will have elevated synaptic modification threshold to support metaplastic synaptic depression, while others that have concurrent Pin1 signaling would be protected from such depression. Metaplasticity has been implicated in selective weakening and strengthening of eye-specific inputs accompanying monocular deprivation (Cooper and Bear, 2012). Our results suggest that metaplasticity may be widely adopted *in vivo* where distinct inputs with different levels of activity converge onto a postsynaptic neuron.

STAR Methods

Lead Contact and Materials Availability

Further information and requests for resources and reagents should be directed to and will be fulfilled by the Lead Contact, Hey-Kyoung Lee (heykyounglee@jhu.edu). This study did not generate new unique reagents.

Experimental model and subject details

Mice—Male and female mice were reared in a 12hr light/12hr dark cycle. Knockout mice for Homer1a (H1aKO), as well as mice with knockin mutations on the TS amino acids (T1123A and S1126A) in the C-terminus of mGluR5 (TSKI) or knockin mutation on the F1128R amino acids in the C-terminus of mGluR5 (FRKI) were obtained from Dr. Paul Worley's lab (Johns Hopkins School of Medicine, Baltimore). Each mutant line was crossed with C57BL/6 mice (The Jackson Laboratory, RRID:IMSR_JAX:000664) to generate wild-type controls termed H1aWT, TSWT, and FRWT, respectively. The floxed-Homer1 ($Homer1^{fl/fl}$) line was also obtained from the Worley lab. To create the conditional knockout for Homer1a with the normal long form of Homer1, we created the H1aKOflox line ($H1b^{fl/+};H1a^{fl/-}$) by crossing $Homer1^{fl/fl}$ with H1aKO. H1aWTflox mice ($H1b^{fl/+};H1a^{fl/+}$) were generated by breeding $Homer1^{fl/fl}$ mice with H1aWT mice. Young animals were dark exposed (DE) between postnatal day 21 (P21) and 35 (P35) for 2 days. DE animals were cared for in the dark room with infrared vision goggles using dim infrared light. Some DE mice were re-exposed to normal light conditions for two hours to study the effects of light exposure (LE).

Layer 4-Cre mice (B6;C3-Tg(Scnn1a-cre)3Aibs/J; The Jackson Laboratory, RRID:IMSR_JAX:009613) were used to study the FF synaptic inputs onto L2/3 cells (L4-Cre). To study the effect of the mGluR5 F1128R mutation on individual inputs, we generated L4-Cre;FRKI mice by crossing L4-Cre mice with FRKI mice. These animals were

dark exposed for two days between P70 and P120 to accommodate sufficient expression of ChR2 in L4 neurons as required for our studies (see *Viral transfections* section for details).

For the mGluR5, mGluR1, and NMDAR pharmacological inhibition studies, C57BL/6 mice (The Jackson Laboratory) were injected intraperitoneally (i.p.) with an equal volume of a given drug or the vehicle solution (filter sterilized phosphate buffered saline, PBS, 10 mM PO_4^{3-}, 137 mM NaCl, and 2.7 mM KCl, pH 7.4) used to dissolve the drug. MPEP hydrochloride (MPEP, 10 mg/kg, Tocris - 1212) was used to block mGluR5, whereas mGluR1 was blocked either with AIDA (1 mg/kg, Tocris - 0904) or Bay36-7620 (20 mg/kg, Tocris - 2501). (R)-CPPene (CPP, 10 mg/kg, Abcam - ab120232) was administered to block NMDARs. The normal reared group was treated 2 hours before collection of slices. DE mice were injected 2 hours before they were dark exposed and received an injection once daily. Mice in the LE group were injected 30 mins before bringing them to light.

All experiments were done in accordance with protocols approved by the Johns Hopkins University Institutional Animal Care and Use Committee (IACUC).

Method details

Viral transfections—Male and female mice were anesthetized in an induction chamber with 3% isoflurane in oxygen (flow rate: 1.0 L/min). L4-Cre mice (B6;C3- Tg(Scnn1a-cre)3Aibs/J; The Jackson Laboratory, RRID:IMSR_JAX:009613) were bilaterally injected in V1 L4 with a double-floxed Channelrhodopsin-2-expressing virus (AAV9.EF1.dflox.hChR2(H134R)-mCherry.WPRE.hGH or AAV9.EF1a.DIO.hChR2(H134R).EYFP.WPRE.HGHpA, Penn Vector Core, University of Pennsylvania: catalog# Addgene20297, Addgene20298, respectively) between P21 and P50. The coordinates of injection relative to Bregma were Lateral: 2.5 mm, Posterior: 3.6 mm, and Depth: 0.45 mm. The virus was allowed to incubate for at least 6 weeks post-injection prior to conducting experiments.

H1aKOflox or H1aWTflox mice (Worley lab) were bilaterally injected in V1 L2/3 with either a Cre-expressing virus (AAV9.CamKII.HI.eGFP-Cre.WPRE.SV40, Penn Vector core Cat# AV-9-PV2521) to knockout the floxed Homer1 hemi-gene or a control enhanced GFP (AAV9.CamKII0.4.eGFP.WPRE.Rbg, Penn Vector core Cat# AV-9-PV1917) vector at P21-30. The coordinates of injection relative to Bregma were Lateral: 2.5 mm, Posterior: 3.6 mm, and Depth: 0.36 mm. Mice recovered on a heating pad after surgery and were returned to the animal colony.

Acute slice preparation—Mice were anesthetized with isoflurane, and decapitation was performed after checking for the absence of a toe-pinch response. Brain blocks containing visual cortex were coronally sectioned into 300 μm sections using a microslicer (Leica Cat#VT1200S or TedPella Pelco easislicer™ Cat#11000). During sectioning, blocks were submerged in ice-cold dissection buffer containing 212.7 mM sucrose, 10 mM dextrose, 3 mM $MgCl_2$, 1 mM $CaCl_2$, 2.6 mM KCl, 1.23 mM $NaH_2PO_4.H_2O$, and 26 mM $NaHCO_3$, which was bubbled with a 95% O_2/5% CO_2 gas mixture. The slices collected from juvenile animals (P21-P45) were incubated at room temperature for 60 mins in an artificial cerebrospinal fluid (ACSF) solution containing 124 mM NaCl, 5 mM KCl, 1.25 mM

$NaH_2PO_4.H_2O$, 26 mM $NaHCO_3$, 10 mM dextrose, 2.5 mM $CaCl_2$, and 1.5 mM $MgCl_2$, which was bubbled with 95% O_2/5% CO_2. The slices collected from older animals (P70-P120) were incubated in the same ACSF solution at 30°C for 30 mins, followed by 30 mins of incubation at room temperature.

Whole cell recording of mEPSCs—Coronal slices were transferred to a recording chamber mounted on the fixed stage of an upright microscope with oblique infrared (IR) illumination. ACSF was continually perfused through the recording chamber, and pH was maintained by bubbling 95% O_2/5% CO_2 gas through the ACSF solution reservoir. AMPA receptor-mediated excitatory postsynaptic currents were isolated by adding 1 μM tetrodotoxin (TTX, Abcam Cat# ab120055), 20 μM (−)-bicuculline methiodide (Bic, Enzo Cat# BML-EA149-0050), and 100 μM DL-2-amino-5-phosphonopentanoic acid (APV, Sigma-Aldrich Cat# A5282) to the ACSF. Recording electrodes were filled with an internal solution containing the following ingredients: 130 mM Cs-gluconate, 10 mM HEPES, 8 mM KCl, 1 mM EGTA, 4 mM Disodium-ATP (Sigma-Aldrich Cat# A6419), 10 mM Disodium-phosphocreatine (Sigma-Aldrich Cat# P7936), 0.5 mM Sodium-GTP (Sigma-Aldrich Cat# G8877), 5 mM Lidocaine N-ethyl bromide (Sigma-Aldrich Cat# L5783) and pH 7.2. Biocytin (1 mg/ml, Sigma-Aldrich Cat# B4261) was added to the internal solution to confirm morphology and location of the recorded cells *post hoc.* Cells were recorded in voltage clamp at −80 mV and the recorded mEPSCs were digitized at 10-kHz by a National Instruments data acquisition board (National instruments Cat# 779556-01, MDL# BNC-2090A) and acquired through a custom script (provided by Claudio Elgueta) in Igor program (Wavemetrics, RRID:SCR_000325).

Whole cell recording of evoked Sr^{2+}-mEPSCs—Slices were continually perfused with Sr^{2+}-ACSF containing 124 mM NaCl, 5 mM KCl, 1.25 mM NaH_2PO_4, 26 mM $NaHCO_3$, 10 mM dextrose, 4mM $SrCl_2$ and 4 mM $MgCl_2$, which was bubbled with 95% O_2/5% CO_2. During recording, cells were held at −80 mV in the presence of 20 μM Bic and 100 μM APV to isolate evoked AMPA receptor currents. Evoked currents were recorded for 10 mins using a custom-made acquisition script (provided by Claudio Elgueta) in Igor program (Wavemetrics, RRID:SCR_000325). Data were acquired every 10 s for a duration of 1,500 ms each. ChR2 expressing L4 inputs were activated 710 ms after the onset of acquisition with 455 nm (5 ms duration) light provided by a light-emitting diode (LED, ThorLabs, M455L3-C5) through a 40x objective lens (Nikon instruments CFI fluor 40X/0.80W). Neighboring L2/3 cells were stimulated electrically by placing a bipolar electrode lateral to the recording site in L2/3. The stimulation current was controlled by digital stimulator (Cygnus Technology Inc. Cat# PG-4000A) and stimulation isolation unit (SIU91A, Cygnus Technology Inc.). The recorded traces were digitized at 10 kHz by a National instruments data acquisition board.

Steady-state surface biotinylation—Biotinylation was performed as previously reported (Goel et al., 2011). Visual cortical slices (400 μm) were prepared as above and further microdissection was done to isolate V1 L2/3 sections. At least 8 slices were collected from each animal. Slices were allowed to recover at room temperature for 30 mins, followed by 30 mins at 30°C in ACSF containing 124 mM NaCl, 5 mM KCl, 1.25 mM

$NaH_2PO_4.H2_O$, 26 mM $NaHCO_3$, 10 mM dextrose, 2.5 mM $CaCl_2$, and 1.5 mM $MgCl_2$, which was bubbled with 95% O_2/5% CO_2. Following recovery, slices were incubated for 10 mins in ice-cold, oxygenated ACSF, followed by 10 mins of incubation in EZ-Link™ Sulfo-NHS-SS-Biotin (2 mg/ml, Thermo Fisher Scientific Cat# 21331) in oxygenated ACSF. The slices then went through 4 rounds of washing (1 min each) with 100 mM Glycine in a Tris-buffered solution (5 mM Tris base, 0.9%NaCl, pH7.4). Finally, the slices were rapidly frozen over dry ice and stored at −80°C.

Separation of the biotinylated surface proteins from internal proteins was performed in a 0.02% SDS and 1% Triton X-100 immunoprecipitation buffer solution (IPB; in mM: 20 mM Na_3PO_4, 150 mM NaCl, 10 mM EDTA, 10 mM EGTA, 10 mM $Na_4P_2O_7$, 50 mM NaF, and 1 mM Na_3VO_4, pH 7.4; with 1 μM okadaic acid and 10 kIU/ml aprotinin). Biotinylated slices were homogenized with ~30 strokes from mechanical glass-teflon tissue homogenizers (Pyrex), and then incubated at 4°C for 30 mins. The homogenized proteins were then separated by centrifugation at 4°C for 10 min at 13,200 rpm and the supernatant was collected in separate tubes. The protein concentration was measured for each of the samples using a BCA protein assay kit (Pierce Cat# 23225) and then normalized to 1 mg/ml. Some of the samples were stored by adding a gel sample buffer as an input for calculating total protein concentration. 300 μg of each sample was mixed with Neutravidin beads (1:1 slurry with 1% TX-IPB, Thermo Fisher Scientific Cat# 53150) and rotated for 2 hours at 4°C. The supernatant containing the intracellular fraction was separated from the beads, by carefully pipetting it into a separate tube. The beads were then washed 3 times with 1% TX-IPB, 3 times with 500 nM NaCl in 1% TX-IPB, and then twice with 1% TX-IPB. The biotinylated surface proteins were eluted with a gel sample buffer and passed through cellulose 0.45 μm Spin-X® acetate centrifuge tube filters (Costar Cat#8163). The input (total population), supernatant (internal proteins), and biotin (surface population) protein groups were run on an 6% SDS-PAGE gel and transferred to PVDF membranes (Biorad 0.45 μm pore size, Cat# 162-0264) for immunoblot analysis.

Immunoblot analysis—Immunoblot analysis for the total and surface population was performed separately for each genotype. An equal quantity of each sample was added (10 μg for total and 90 μg for surface proteins), separated on a 6% SDS-PAGE gel, and transferred to a PVDF membrane (0.45 μm pore size, Biorad Cat# 162-0264). The transferred samples were treated with blocking buffer containing 1% bovine serum albumin (BSA, Fisher Scientific Cat#BP1600-1) in PBST (0.1% Tween-20, 10 mM PO_4^{3-}, 137 mM NaCl, and 2.7 mM KCl, pH 7.4) for one hour at room temperature. Primary antibodies against GluA1 (1:500, Rabbit polyclonal, Millipore Cat# AB1504, RRID# AB_2113602), GluA2 (1:200, Mouse, Millipore Cat# MAB397, RRID:AB_2113875), mGluR5 (1:500, Rabbit, Millipore Cat# AB5675, RRID:AB_2295173), NR1 (1:500, Rabbit, obtained from Dr. Richard Huganir's lab, Johns Hopkins School of Medicine, Baltimore), NR2A (3:1000, Rabbit, Millipore Cat# 07-632, RRID:AB_310837), NR2B (3:500, Rabbit, Thermo Fisher Scientific Cat# 71-8600, RRID:AB_2534001) and Tubulin (1:500, Millipore Cat# 05-559, RRID:AB_309804) diluted in the blocking buffer were applied for one hour at room temperature. Following four washes with the blocking buffer, membranes were treated with either ECL-plex conjugated with Cy dyes (GluA1 and mGluR5: goat anti-rabbit Cy5, GE

Healthcare Cat# PA45011, RRID:AB_772205; GluA2: goat anti-mouse Cy3, GE Healthcare Cat# PA43010, RRID:AB_772196; Tubulin: goat anti-mouse Cy5, GE Healthcare Cat# PA45010, RRID:AB_772198) or anti-rabbit alkaline phosphatase-tagged secondary antibodies (NR1, NR2A and NR2B: Thermo Fisher Scientific Cat# 31340, RRID:AB_228339) for one hour at room temperature. In case of alkaline phosphatase antibodies, ECF substrate (GE Healthcare Cat# RPN5785) was applied after 4 washes with the blocking buffer for 20 mins. The membranes were imaged using Typhoon 9410 molecular imager (GE Healthcare Cat# 8149-30-9410).

For H1b/c and Tubulin immunoblot analysis, 20 μg each of H1aWT and H1aKO samples were run on a 12% SDS-PAGE gels and transferred to an Immobilon-P PVDF membrane (0.20 μm pore size, Millipore Cat# ISEQ00010). Primary antibody (obtained from Dr. Paul Worley's lab, Johns Hopkins School of Medicine, 1:500 dilution) for the EVH domain of Homer1 recognized H1b/c at 48kDa. Membranes were treated in the same manner as mentioned above to probe for H1b/c and Tubulin. ECL-plex conjugated with Cy dyes were used as secondary antibody (H1b/c: goat anti-rabbit Cy5, GE Healthcare Cat# PA45011, RRID:AB_772205; Tubulin: goat anti-mouse Cy3, GE Healthcare Cat# PA43010, RRID:AB_772196). A Typhoon 9410 molecular imager was used to image the membranes (GE healthcare Cat# 8149-30-9410).

Biocytin processing for confirmation of mEPSC recordings in GFP-expressing cells—Slices containing recorded cells were fixed in pre-made formalin solution (Sigma Aldrich Cat# HT5014; MDL: MFCD00003274) overnight at 4°C. Slices were washed twice for 10 mins at room temperature in 0.1 mM phosphate buffer (PB) composed of 19 mM $NaH_2PO_4H_2O$ and 81 mM Na_2HPO_4. The slices were then permeabilized in 2% Triton X-100 (Fisher Scientific Cat# BP151-100) in 0.1 mM PB for 1 hour and later incubated overnight at 4°C in an avidin-Texas Red conjugate (Thermo Fisher Scientific Cat# A820) diluted 1:2000 in 1% Triton X-100 (in 0.1 M PB) and shielded from light. After the avidin incubation, slices were rinsed twice with 0.1M PB, mounted on glass slides, and allowed to air dry for 20 mins in the dark. Slides were cover-slipped with Prolong Anti-fade (Invitrogen Cat# P36930) mounting medium and sealed with nail polish. Images were taken using an LSM 510 META confocal microscope (Zeiss).

Quantitative polymerase chain reaction (qPCR)—V1 slices (400 μm) were obtained from the animals as explained in acute slice preparation section above. V1 L2/3 was isolated by performing micro-dissections. The slices were quickly frozen on dry ice and stored for mRNA separation. The total RNA content was separated from collected V1 slices using TRIzol-chloroform extraction (ThermoFisher Cat# 10296-010). cDNA was obtained from RNA using the RETROscript Reverse Transcription kit (ThermoFisher Cat# AM1710). For quantification, real-time qPCR was performed using a Maxima SYBR Green/Rox Q-PCR Master Mix (ThermoFisher Cat# K0221), in a StepOnePlusTM Real-Time PCR system (Applied Biosystems Cat# 4376600; RRID:SCR_015805). The following primer sequences were used for each gene:

H1a: forward primer (FP) 5′-CCAGAAAGTATCAATGGGACAGATG-3′; reverse primer (RP) 5′-TGCTGAATTGAATGTGTACCTATGTG-3′

H1b/c: FP 5'-GGCAAACACTGTTTATGGACTGG-3'; RP 5'-CTCTGTTCTTGGAGTTCTCTGGC-3'

GFP: FP 5′-GGTCTTGTAGTTGCCGTGT-3′; RP 5′-CCTGAAGTTCATCTGCACCA-3′

GAPDH: FP 5′-CTGGAGAAACCTGCCAAGTA-3′; 5′-AGTGGGAGTTGCTGTTGAAG-3′

Quantification and statistical analysis

Quantification of mEPSCs events was performed using Mini Analysis Software (Synaptosoft, RRID:SCR_002184) and 200 isolated events from each cell were quantified.

For quantification of Sr^{2+}-mEPSCs, the amplitude and frequency of pre-stimulus events (spontaneous events) were measured in a window spanning 200 ms to 650 ms from the beginning of acquisition. The stimulation pulse was given at 710 ms, and post-stimulus events (evoked events) were measured from 760 to 1160 ms. At least 50 events on each group were analyzed to determine an average frequency (Pre_{freq} and $Post_{freq}$) and amplitude (Pre_{amp} and $Post_{amp}$) using Mini Analysis Program (Synaptosoft, RRID:SCR_002184). Cells were determined to have desynchronized events if their $Post_{freq}$ was higher than their Pre_{freq} by at least 2-Hz. The average evoked amplitude and average traces were calculated to subtract the spontaneous events using this formula:

$$\frac{Post_{amp} x Post_{freq} - Pre_{amp} x Pre_{freq}}{Post_{freq} - Pre_{freq}}$$

Western blots results were visualized and analyzed using ImageQuant TL 7.0 software (ImageQuant, RRID:SCR_014246). QPCR data was analyzed with StepOne Software (StepOne Software, RRID:SCR_014281) using the $\Delta\Delta C_t$ method normalized to GAPDH readings for each sample. H1a, H1b/c, and GFP mRNA levels in the test groups were quantified as a fold increase of the wild-type group.

All statistical analysis was performed using Graphpad PRISM software (Graphpad Prism, RRID:SCR_002798). The D'Agostino and Pearson omnibus normality test was used to check for normality. For datasets that passed the normality test, oneway ANOVA was performed with the Newman-Keuls multiple comparison *posthoc* test was used for comparison of more than two groups. MEPSC frequency for the LE group of H1aWT mice did not pass the normality test. Hence, the Kruskal-Wallis test was performed to determine the effect of visual experience on mEPSC frequency in H1aWT. For comparisons between two groups of normally distributed data the Student's t-test was used. Cumulative probability distributions were compared between two distributions using the non-parametric Mann-Whitney test. Data plots were made using Python and Microsoft Excel. Bar graphs display mean ± SEM (standard error of mean). Estimated population density plots were generated by calculating the probability of distribution by fitting the Gaussian kernel for each measured data point.

Data and Code availability

All the datasets are available upon request. All the software and algorithms have been either commercially available or custom scripts generated by a source listed under each subsection above. Custom scripts for data acquisition and analysis are available upon request.

Supplementary Material

Refer to Web version on PubMed Central for supplementary material.

Acknowledgements

This work was supported by NIH grants R01-EY014882 to H.-K.L and DA010309 to P.F.W. Authors would like to thank Dr. Alfredo Kirkwood for helpful discussions on this project, and Dr. Rejji Kuruvilla for help on qPCR experiments.

References

Abbott LF, and Nelson SB (2000). Synaptic plasticity: taming the beast. Nature neuroscience 3 Suppl, 1178–1183. [PubMed: 11127835]

Abdul-Ghani MA, Valiante TA, and Pennefather PS (1996). Sr2+ and quantal events at excitatory synapses between mouse hippocampal neurons in culture. J Physiol 495 (Pt 1), 113–125. [PubMed: 8866356]

Abraham WC (2008). Metaplasticity: tuning synapses and networks for plasticity. Nature reviews Neuroscience 9, 387. [PubMed: 18401345]

Ango F, Pin JP, Tu JC, Xiao B, Worley PF, Bockaert J, and Fagni L (2000). Dendritic and axonal targeting of type 5 metabotropic glutamate receptor is regulated by homer1 proteins and neuronal excitation. The Journal of neuroscience 20, 8710–8716. [PubMed: 11102477]

Ango F, Prézeau L, Muller T, Tu JC, Xiao B, Worley PF, Pin JP, Bockaert J, and Fagni L (2001). Agonist-independent activation of metabotropic glutamate receptors by the intracellular protein Homer. Nature 411, 35082096.

Ballester-Rosado CJ, Albright MJ, Wu CS, Liao CC, Zhu J, Xu J, Lee LJ, and Lu HC (2010). mGluR5 in cortical excitatory neurons exerts both cell-autonomous and -nonautonomous influences on cortical somatosensory circuit formation. The Journal of neuroscience : the official journal of the Society for Neuroscience 30, 16896–16909. [PubMed: 21159961]

Barnes SJ, Franzoni E, Jacobsen RI, Erdelyi F, Szabo G, Clopath C, Keller GB, and Keck T (2017). Deprivation-Induced Homeostatic Spine Scaling In Vivo Is Localized to Dendritic Branches that Have Undergone Recent Spine Loss. Neuron 96, 871–882 e875. [PubMed: 29107520]

Bear MF, Cooper LN, and Ebner FF (1987). A physiological basis for a theory of synapse modification. Science 237, 42–48. [PubMed: 3037696]

Beique JC, Na Y, Kuhl D, Worley PF, and Huganir RL (2011). Arc-dependent synapse-specific homeostatic plasticity. Proceedings of the National Academy of Sciences of the United States of America 108, 816–821. [PubMed: 21187403]

Bienenstock EL, Cooper LN, and Munro PW (1982). Theory for the development of neuron selectivity: orientation specificity and binocular interaction in visual cortex. The Journal of neuroscience : the official journal of the Society for Neuroscience 2, 32–48. [PubMed: 7054394]

Binzegger T, Douglas RJ, and Martin KA (2004). A quantitative map of the circuit of cat primary visual cortex. The Journal of neuroscience : the official journal of the Society for Neuroscience 24, 8441–8453. [PubMed: 15456817]

Bortolotto ZA, Bashir ZI, Davies CH, and Collingridge GL (1994). A molecular switch activated by metabotropic glutamate receptors regulates induction of long-term potentiation. Nature 368, 740–743. [PubMed: 8152485]

Brakeman PR, Lanahan AA, O'Brien R, Roche K, Barnes CA, Huganir RL, and Worley PF (1997). Homer: a protein that selectively binds metabotropic glutamate receptors. Nature 386, 284–288. [PubMed: 9069287]

Bridi MCD, de Pasquale R, Lantz CL, Gu Y, Borrell A, Choi SY, He K, Tran T, Hong SZ, Dykman A, et al. (2018). Two distinct mechanisms for experience-dependent homeostasis. Nature neuroscience 21, 843–850. [PubMed: 29760525]

Cavarsan CF, Matsuo A, Blanco MM, and Mello LE (2015). Maximal electroshock-induced seizures are able to induce Homer1a mRNA expression but not pentylenetetrazole-induced seizures. Epilepsy Behav 44, 90–95. [PubMed: 25659045]

Cavarsan CF, Tescarollo F, Tesone-Coelho C, Morais RL, Motta FL, Blanco MM, and Mello LE (2012). Pilocarpine-induced status epilepticus increases Homer1a and changes mGluR5 expression. Epilepsy Res 101, 253–260. [PubMed: 22591751]

Cohen AS, and Abraham WC (1996). Facilitation of long-term potentiation by prior activation of metabotropic glutamate receptors. Journal of neurophysiology 76, 953–962. [PubMed: 8871210]

Conn PJ, and Pin JP (1997). Pharmacology and functions of metabotropic glutamate receptors. Annu Rev Pharmacol Toxicol 37, 205–237. [PubMed: 9131252]

Cooper LN, and Bear MF (2012). The BCM theory of synapse modification at 30: interaction of theory with experiment. Nature reviews Neuroscience 13, 798–810. [PubMed: 23080416]

Dantzker JL, and Callaway EM (2000). Laminar sources of synaptic input to cortical inhibitory interneurons and pyramidal neurons. Nature neuroscience 3, 701–707. [PubMed: 10862703]

Dodge FA Jr., Miledi R, and Rahamimoff R (1969). Strontium and quantal release of transmitter at the neuromuscular junction. J Physiol 200, 267–283. [PubMed: 4387376]

Douglas RJ, and Martin KA (2004). Neuronal circuits of the neocortex. Annu Rev Neurosci 27, 419–451. [PubMed: 15217339]

Gao M, Sossa K, Song L, Errington L, Cummings L, Hwang H, Kuhl D, Worley P, and Lee HK (2010). A specific requirement of Arc/Arg3.1 for visual experience-induced homeostatic synaptic plasticity in mouse primary visual cortex. The Journal of neuroscience : the official journal of the Society for Neuroscience 30, 7168–7178. [PubMed: 20505084]

Gil Z, Connors BW, and Amitai Y (1999). Efficacy of thalamocortical and intracortical synaptic connections: quanta, innervation, and reliability. Neuron 23, 385–397. [PubMed: 10399943]

Gil-Sanz C, Delgado-Garcia JM, Fairen A, and Gruart A (2008). Involvement of the mGluR1 receptor in hippocampal synaptic plasticity and associative learning in behaving mice. Cerebral cortex 18, 1653–1663. [PubMed: 18024992]

Goel A, Jiang B, Xu LW, Song L, Kirkwood A, and Lee HK (2006). Cross-modal regulation of synaptic AMPA receptors in primary sensory cortices by visual experience. Nature neuroscience 9, 1001–1003. [PubMed: 16819524]

Goel A, and Lee HK (2007). Persistence of experience-induced homeostatic synaptic plasticity through adulthood in superficial layers of mouse visual cortex. The Journal of neuroscience : the official journal of the Society for Neuroscience 27, 6692–6700. [PubMed: 17581956]

Guo Y, Huang S, de Pasquale R, McGehrin K, Lee HK, Zhao K, and Kirkwood A (2012). Dark exposure extends the integration window for spike-timing-dependent plasticity. The Journal of neuroscience : the official journal of the Society for Neuroscience 32, 15027–15035. [PubMed: 23100424]

Hu J-HH, Park JM, Park S, Xiao B, Dehoff MH, Kim S, Hayashi T, Schwarz MK, Huganir RL, Seeburg PH, et al. (2010). Homeostatic scaling requires group I mGluR activation mediated by Homer1a. Neuron 68, 1128–1142. [PubMed: 21172614]

Iurilli G, Ghezzi D, Olcese U, Lassi G, Nazzaro C, Tonini R, Tucci V, Benfenati F, and Medini P (2012). Sound-driven synaptic inhibition in primary visual cortex. Neuron 73, 814–828. [PubMed: 22365553]

Kammermeier PJ, and Worley PF (2007). Homer 1a uncouples metabotropic glutamate receptor 5 from postsynaptic effectors. Proc Natl Acad Sci U S A 104, 6055–6060. [PubMed: 17389377]

Kammermeier PJ, Xiao B, Tu JC, Worley PF, and Ikeda SR (2000). Homer proteins regulate coupling of group I metabotropic glutamate receptors to N-type calcium and M-type potassium channels. J Neurosci 20, 7238–7245. [PubMed: 11007880]

Kato N (2009). Neurophysiological mechanisms of electroconvulsive therapy for depression. Neuroscience Research 64, 3–11. [PubMed: 19321135]

Kim CH, Braud S, Isaac JT, and Roche KW (2005). Protein kinase C phosphorylation of the metabotropic glutamate receptor mGluR5 on Serine 839 regulates Ca2+ oscillations. The Journal of biological chemistry 280, 25409–25415. [PubMed: 15894802]

Lopez-Bendito G, Shigemoto R, and Fairen A (2002). Differential distribution of group I metabotropic glutamate receptors during rat cortical development. Cerebral cortex.

Luo P, Chen T, Zhao Y, Zhang L, Yang Y, Liu W, Li S, Rao W, Dai S, Yang J, and Fei Z (2014). Postsynaptic scaffold protein Homer 1a protects against traumatic brain injury via regulating group I metabotropic glutamate receptors. Cell death & disease 5.

Marton TM, Hussain Shuler MG, and Worley PF (2015). Homer 1a and mGluR5 phosphorylation in reward-sensitive metaplasticity: A hypothesis of neuronal selection and bidirectional synaptic plasticity. Brain Res 1628, 17–28. [PubMed: 26187757]

Matta JA, Ashby MC, Sanz-Clemente A, Roche KW, and Isaac JTR (2011). mGluR5 and NMDA receptors drive the experience- and activity-dependent NMDA receptor NR2B to NR2A subunit switch. Neuron 70, 339–351. [PubMed: 21521618]

Miska NJ, Richter LM, Cary BA, Gjorgjieva J, and Turrigiano GG (2018). Sensory experience inversely regulates feedforward and feedback excitation-inhibition ratio in rodent visual cortex. eLife 7.

Moutin E, Raynaud F, Roger J, Pellegrino E, Homburger V, Bertaso F, Ollendorff V, Bockaert J, Fagni L, and Perroy J (2012). Dynamic remodeling of scaffold interactions in dendritic spines controls synaptic excitability. The Journal of cell biology 198, 251–263. [PubMed: 22801779]

Okada D, Ozawa F, and Inokuchi K (2009). Input-specific spine entry of soma-derived Vesl-1S protein conforms to synaptic tagging. Science 324, 904–909. [PubMed: 19443779]

Okubo Y, Sekiya H, Namiki S, Sakamoto H, Iinuma S, Yamasaki M, Watanabe M, Hirose K, and Iino M (2010). Imaging extrasynaptic glutamate dynamics in the brain. Proc Natl Acad Sci U S A 107, 6526–6531. [PubMed: 20308566]

Oliet SH, Malenka RC, and Nicoll RA (1996). Bidirectional control of quantal size by synaptic activity in the hippocampus. Science 271, 1294–1297. [PubMed: 8638114]

Pagano A, Ruegg D, Litschig S, Stoehr N, Stierlin C, Heinrich M, Floersheim P, Prezèau L, Carroll F, Pin JP, et al. (2000). The non-competitive antagonists 2-methyl-6-(phenylethynyl)pyridine and 7-hydroxyiminocyclopropan[b]chromen-1a-carboxylic acid ethyl ester interact with overlapping binding pockets in the transmembrane region of group I metabotropic glutamate receptors. The Journal of biological chemistry 275, 33750–33758. [PubMed: 10934211]

Park JM, Hu JH, Milshteyn A, Zhang PW, Moore CG, Park S, Datko MC, Domingo RD, Reyes CM, Wang XJ, et al. (2013). A prolyl-isomerase mediates dopamine-dependent plasticity and cocaine motor sensitization. Cell 154, 637–650. [PubMed: 23911326]

Petrus E, Rodriguez G, Patterson R, Connor B, Kanold PO, and Lee HK (2015). Vision Loss Shifts the Balance of Feedforward and Intracortical Circuits in Opposite Directions in Mouse Primary Auditory and Visual Cortices. The Journal of neuroscience : the official journal of the Society for Neuroscience 35, 8790–8801. [PubMed: 26063913]

Philpot BD, Espinosa JS, and Bear MF (2003). Evidence for altered NMDA receptor function as a basis for metaplasticity in visual cortex. The Journal of neuroscience : the official journal of the Society for Neuroscience 23, 5583–5588. [PubMed: 12843259]

Philpot BD, Sekhar AK, Shouval HZ, and Bear MF (2001). Visual experience and deprivation bidirectionally modify the composition and function of NMDA receptors in visual cortex. Neuron 29, 157–169. [PubMed: 11182088]

Quinlan EM, Olstein DH, and Bear MF (1999). Bidirectional, experience-dependent regulation of N-methyl-D-aspartate receptor subunit composition in the rat visual cortex during postnatal development. Proceedings of the National Academy of Sciences of the United States of America 96, 12876–12880. [PubMed: 10536016]

Ronesi JA, Collins KA, Hays SA, Tsai N-PP, Guo W, Birnbaum SG, Hu J-HH, Worley PF, Gibson JR, and Huber KM (2012). Disrupted Homer scaffolds mediate abnormal mGluR5 function in a mouse model of fragile X syndrome. Nature neuroscience 15, 431. [PubMed: 22267161]

Schroeder CE, and Foxe J (2005). Multisensory contributions to low-level, 'unisensory' processing. Current opinion in neurobiology 15, 454–458. [PubMed: 16019202]

Shiraishi-Yamaguchi Y, and Furuichi T (2007). The Homer family proteins. Genome Biology 8, 206. [PubMed: 17316461]

Tappe A, Klugmann M, Luo C, Hirlinger D, Agarwal N, Benrath J, Ehrengruber MU, During MJ, and Kuner R (2006). Synaptic scaffolding protein Homer1a protects against chronic inflammatory pain. Nature Medicine 12, 677–681.

Thomson AM, and Lamy C (2007). Functional maps of neocortical local circuitry. Frontiers in Neuroscience 1, 19–42. [PubMed: 18982117]

Tsanov M, and Manahan-Vaughan D (2009). Synaptic plasticity in the adult visual cortex is regulated by the metabotropic glutamate receptor, mGluR5. Experimental brain research 199, 391–399. [PubMed: 19672584]

Tu JC, Xiao B, Naisbitt S, Yuan JP, Petralia RS, Brakeman P, Doan A, Aakalu VK, Lanahan AA, Sheng M, and Worley PF (1999). Coupling of mGluR/Homer and PSD-95 complexes by the Shank family of postsynaptic density proteins. Neuron 23, 583–592. [PubMed: 10433269]

Tu JC, Xiao B, Yuan JP, Lanahan AA, Leoffert K, Li M, Linden DJ, and Worley PF (1998). Homer binds a novel proline-rich motif and links group 1 metabotropic glutamate receptors with IP3 receptors. Neuron 21, 717–726. [PubMed: 9808459]

Turrigiano GG (2008). The self-tuning neuron: synaptic scaling of excitatory synapses. Cell 135, 422–435. [PubMed: 18984155]

Turrigiano GG, Leslie KR, Desai NS, Rutherford LC, and Nelson SB (1998). Activity-dependent scaling of quantal amplitude in neocortical neurons. Nature 391, 892–896. [PubMed: 9495341]

Wang Y, Rao W, Zhang C, Zhang C, Liu MD, Han F, Yao LB, Han H, Luo P, Su N, and Fei Z (2015). Scaffolding protein Homer1a protects against NMDA-induced neuronal injury. Cell Death Dis 6, e1843. [PubMed: 26247728]

Whitt JL, Petrus E, and Lee HK (2014). Experience-dependent homeostatic synaptic plasticity in neocortex. Neuropharmacology 78, 45–54. [PubMed: 23466332]

Xu X, Olivas ND, Ikrar T, Peng T, Holmes TC, Nie Q, and Shi Y (2016). Primary visual cortex shows laminar specific and balanced circuit organization of excitatory and inhibitory synaptic connectivity. The Journal of physiology.

Yang SN, Tang YG, and Zucker RS (1999). Selective induction of LTP and LTD by postsynaptic [Ca2+]i elevation. J Neurophysiol 81, 781–787. [PubMed: 10036277]

Yang W, Carrasquillo Y, Hooks BM, Nerbonne JM, and Burkhalter A (2013). Distinct balance of excitation and inhibition in an interareal feedforward and feedback circuit of mouse visual cortex. The Journal of neuroscience : the official journal of the Society for Neuroscience 33, 17373–17384. [PubMed: 24174670]

Yee AX, Hsu Y-T, and Chen L (2017). A metaplasticity view of the interaction between homeostatic and Hebbian plasticity. Philosophical Transactions of the Royal Society B: Biological Sciences 372, 20160155.

Highlights

- Visual experience induces input-specific metaplasticity in L2/3 of visual cortex.
- Both NMDAR and mGluR5 are necessary for input-specific metaplasticity.
- mGluR5 and H1a interaction mediates input-specific homeostasis *in vivo.*

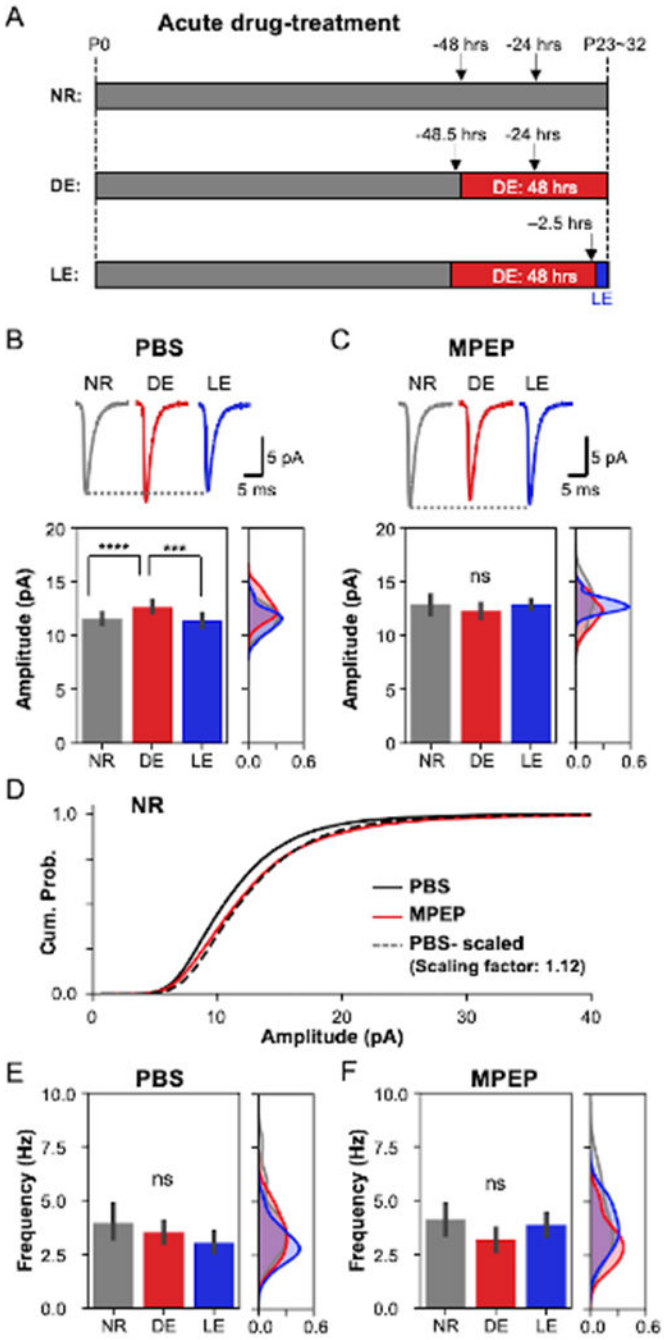

Figure 1. mGluR5 activity is required for experience-dependent downregulation of mEPSCs

(A) Experimental design. Mice were normally reared until opening of the critical period (~P21), then either given PBS or MPEP. For NR and DE conditions, PBS or MPEP (once daily i.p.) were given for 2 days, while for LE condition PBS/MPEP injection was given once after 2 days of DE and 30 min prior to light exposure. Arrows: time of each injection. (B, C) MPEP prevents experience-dependent reduction in mEPSC amplitudes. Top: Average mEPSC traces. Bottom left: Comparison of average mEPSC amplitude (B, PBS: NR=11.6±0.2 pA, n=15; DE=12.65±0.3 pA, n=17; LE=11.4±0.3 pA, n=13; ANOVA,

F(2,42)=6.57, **p<0.01; C, MPEP: NR=12.9±0.4 pA, n=15; DE=12.3±0.3 pA, n=14; LE=12.9±0.2 pA, n=14; ANOVA, F(2,40)=1.074, p=0.35). Bottom right: Estimated population density plot of mEPSC amplitudes. X-axis: Estimated probability density, which is the probability per mEPSC amplitude estimated from each measured data fitted with the Gaussian kernels. Y-axis: shared with the left panel. For MPEP group, there was no significant change in the average mEPSC amplitudes, but a significant difference in the variance of the estimated population density probability (see Table S1) reflecting a change in the variance of mEPSC amplitudes in the population.

(D) MPEP treatment (once daily i.p. for 2 days) in NR mice increases mEPSC amplitude in a multiplicative manner. (Mann-Whitney test: NR-PBS vs. NR-MPEP, p<0.0001; NR-PBS-scaled vs. NR-MPEP, p>0.01)

(E, F) mEPSC frequency does not change across groups. Left: Comparison of average mEPSC frequency (E, PBS: NR=4.0±0.4 Hz, n=15; DE=3.5±0.2 Hz, n=17; LE=3.0±0.2 Hz, n=13; ANOVA, F(2,42)=2.07, p=0.14; F, MPEP: NR=4.1±0.4 Hz, n=15; DE=3.2±0.3 Hz, n=14; LE=3.9±0.3 Hz, n=14; ANOVA, F(2,40)=1.57, p=0.09). ns: Not statistically significant. Right: Estimated population density plot of mEPSC frequencies. X-axis: Estimated probability density, which is the probability per mEPSC frequency estimated from each measured data fitted with the Gaussian kernels.

Also see Figure S1 and Table S1.

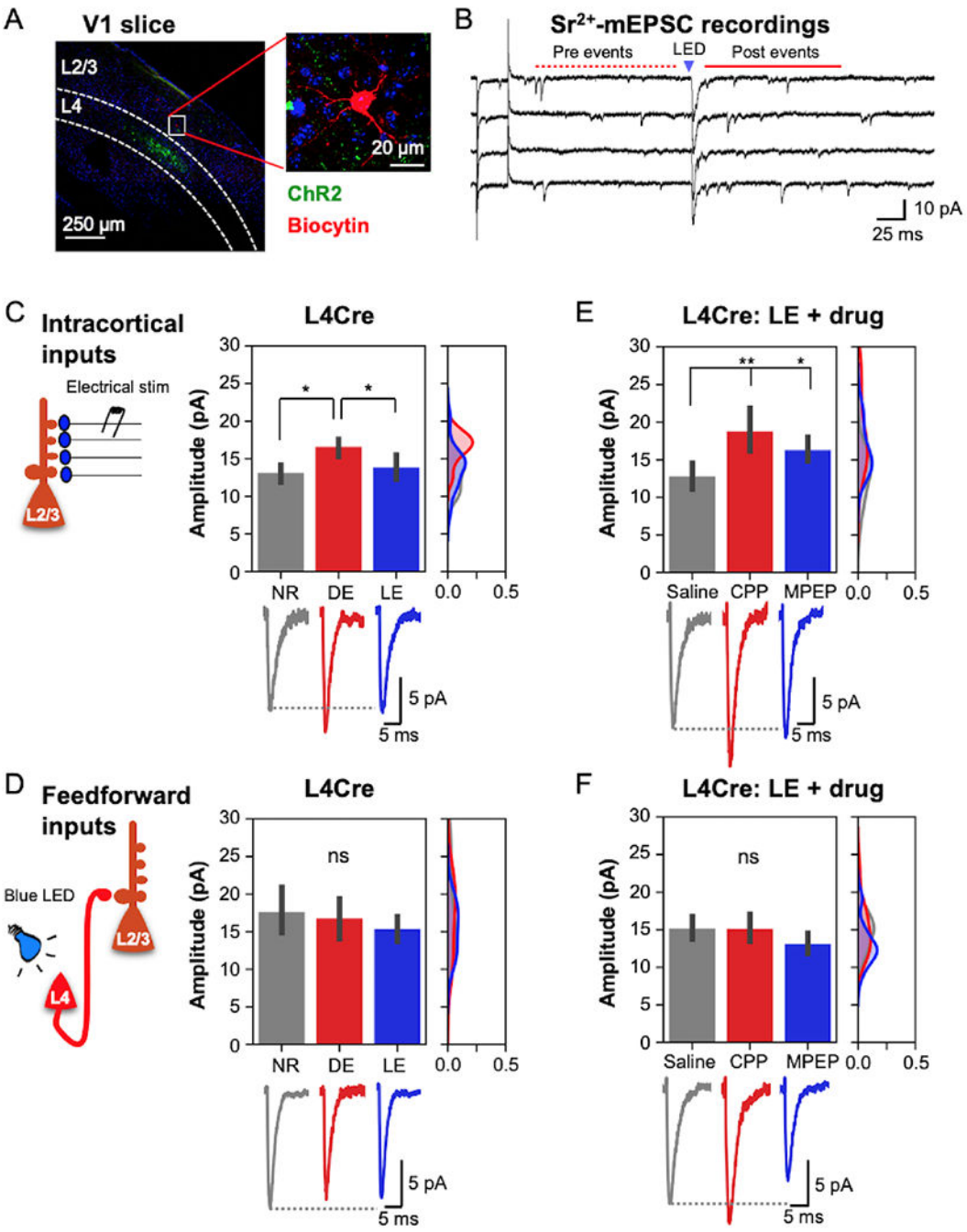

Figure 2. Visual experience produces input-specific weakening of IC inputs to L2/3 neurons requiring NMDAR and mGluR5 activity

L4Cre mice (≥P21) were injected with AAV to express ChR2-tagged with YFP or mCherry in V1 L4 neurons. Virus was incubated for ≥6 weeks and recordings were done at P70-120. (A) Confocal image of a V1 slice used for recording showing ChR2-YFP in L4 (green) and a recorded neuron (red, biocytin filled) in L2/3. Left: lower magnification image. Right: higher magnification image of the L2/3 neuron showing a pyramidal shaped soma (red) and ChR2-YFP axons around (green).

(B) Sr^{2+}-mEPSCs recording example traces. L4 inputs were activated by blue LED stimulation (5 ms duration, blue arrow head). Spontaneous events were recorded before the evoked response during a 450 ms window (red-dashed line). Sr^{2+}-desynchronized LED-evoked events were recorded 50 ms after the evoked response in a 400 ms window (red-solid line). The strength of evoked inputs was calculated by subtracting out the spontaneous events (see STAR methods for details). IC inputs were activated by a stimulating electrode placed laterally in L2/3, and quantified using the same method. (C,D) Changes in visual experience regulate the strength of lateral IC inputs to L2/3 neurons, but not FF inputs from L4. Left: Schematics of the experiment. Lateral IC inputs were activated via electrical stimulation (C), while L4 inputs were activated by ChR2 expression in L4Cre mice (D). Middle: Comparison of calculated average evoked Sr^{2+}-mEPSC amplitude (C, IC inputs: NR=13.1±0.6 pA, n=12; DE=16.2±0.6 pA, n=12; LE=13.8±0.8 pA, n=13; ANOVA, $F(2,34)=5.096$, $p<0.05$; Newman-Keuls multiple comparison *$p<0.05$; D, FF inputs: NR=17.6±1.6 pA, n=13; DE=16.8±1.4 pA, n=12; LE=15.3±0.9 pA, n=13; ANOVA, $F(2,35)=0.5751$, $p>0.72$). Right: Estimated population density plot of Sr^{2+}-mEPSC amplitudes. X-axis, Estimated probability density. Bottom: Average evoked Sr^{2+}-mEPSC traces.

(E,F) LE-induced reduction in lateral IC inputs to L2/3 neurons is dependent on NMDAR and mGluR5. Left: Comparison of calculated evoked Sr^{2+}-mEPSC amplitude from IC inputs (E) and FF inputs (F) to L2/3 neurons of LE mice which received saline, NMDAR antagonist (CPP) or mGluR5 inverse agonist (MPEP) injection 30 min before reexposure to light following 2 days of DE (E, IC inputs: LE+Saline=12.8±0.9 pA, n=12; LE +CPP=18.2±1.4 pA, n=12; LE+MPEP=16.1±0.8 pA, n=15; ANOVA, $F(2,36)=6.411$, $p<0.01$; Newman-Keuls multiple comparison **$p<0.01$, *$p<0.05$; F, FF inputs: LE +Saline=15.2±0.8 pA, n=12; LE+CPP=15.11±1.0 pA, n=13; LE+MPEP=13.1±0.7 pA, n=17; ANOVA, $F(2,39)=2.304$, $p>0.11$). Right: Estimated population density plot of Sr^{2+}-EPSC amplitudes. X-axis, Estimated probability density. Bottom: Average evoked Sr^{2+}-mEPSC traces.

Also see Table S1.

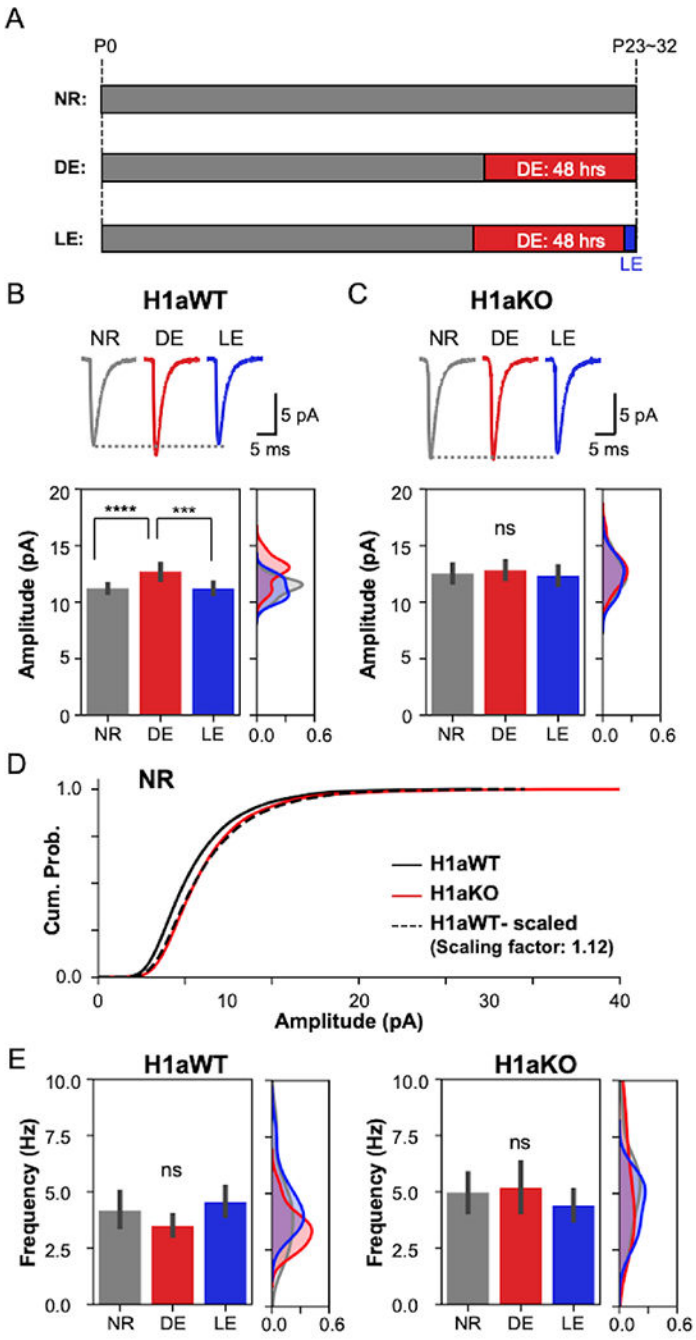

Figure 3. H1aKOs lack visual experience-dependent synaptic weakening in V1 L2/3 neurons

(A) Schematics of the experiments. H1aWT and H1aKO mice were reared normally until P21~P30. A group of mice were put in the darkroom for 2 days (DE), and another group of mice underwent the same 2 day DE followed by 2 hours LE.

(B,C) H1aKO lack experience-dependent regulation of mEPSCs. Top: Average mEPSC traces. Bottom left: Comparison of average mEPSC amplitude (B, H1aWT: NR=11.2±0.2 pA, n=20; DE=12.7±0.3 pA, n=14; LE=11.2±0.2 pA, n=14; ANOVA, F(2,45)=11.07, p=0.0001; Newman-Keuls multiple comparison ***p<0.001, ****p<0.0001; C, H1aKO:

NR=12.5±0.4 pA, n=15; DE=12.8±0.4 pA, n=14; LE=12.3±0.4 pA, n=12; ANOVA, F(2,38)=0.4, p=0.67). Bottom right: Estimated population density plot of mEPSC amplitudes. X-axis, Estimated probability density.

(D) Cumulative probability graph plotting mEPSC amplitudes from NR H1aKO (blue solid line) and NR H1aWT (black solid line) are statistically significantly different while H1aWT mEPSC amplitudes that are scaled up by a scaling factor (1.12) is not different from those of H1aKOs (Mann-Whitney test: NR-H1aWT vs. NR-H1aKO, $p<0.0001$; NR-H1aWT-scaled vs. NR-H1aKO, $p>0.4$).

(E) No change in average mEPSC frequency. First panel: Comparison of average mEPSC frequency of H1aWTs (NR=4.2±0.4 Hz, n=20; DE=3.5±0.2 Hz, n=14; LE=4.6±0.3 Hz, n=14; Kruskal-Wallis test, $p>0.09$). Second panel: Estimated population density plots of mEPSC frequency (X-axis, Estimated probability density). Third panel: Comparison of average mEPSC frequency of H1aKOs (NR=5.0±0.4 Hz, n=15; DE=5.2±0.6 Hz, n=14; LE=4.4±0.3 Hz, n=12; ANOVA, F(2,38)=0.65, p=0.53). Fourth panel: Estimated population density plots (X-axis, Estimated probability density).

Also see Figure S2 and S3; Table S1.

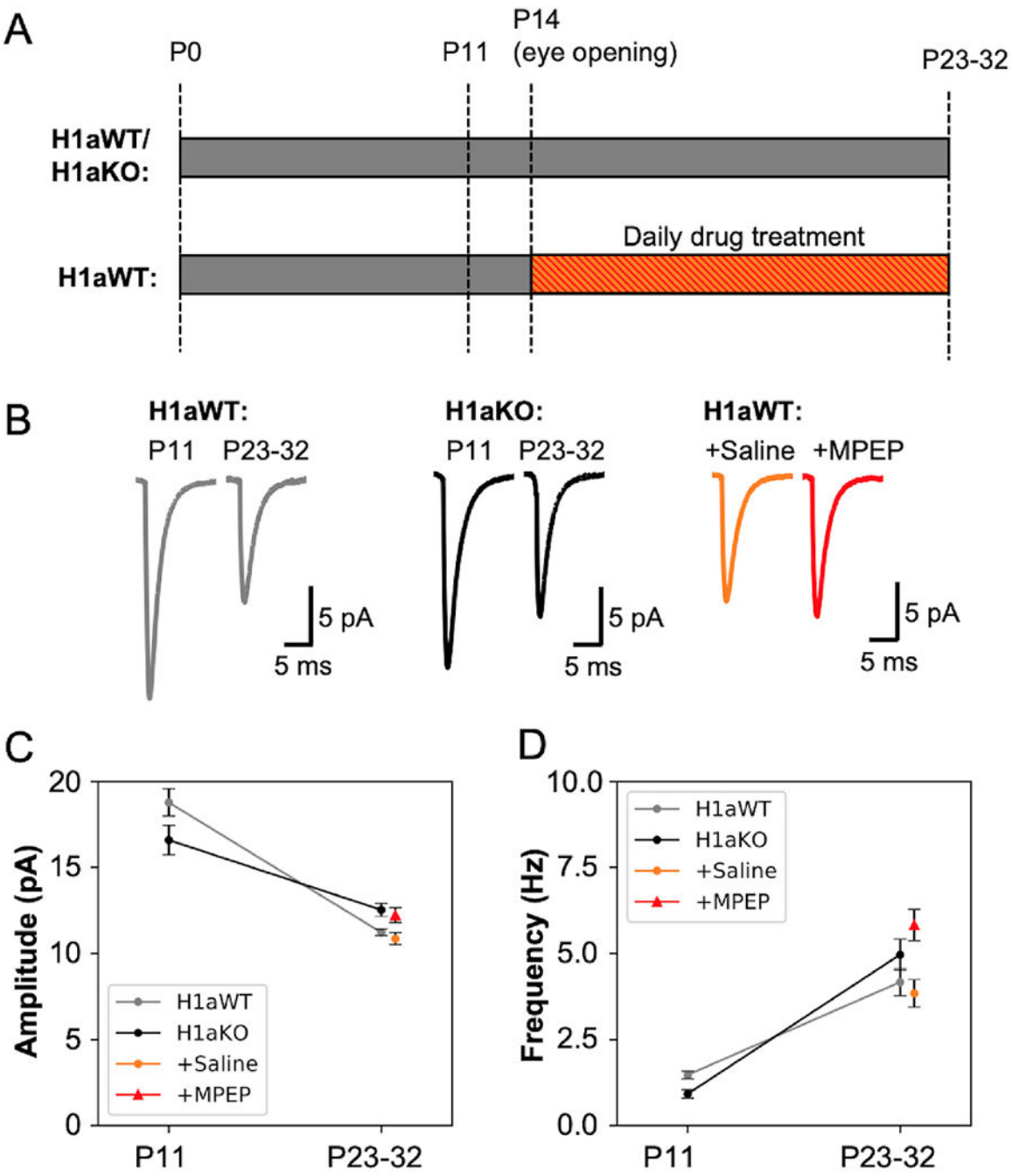

Figure 4. H1a knockout does not grossly alter developmental changes in mEPSCs of V1 L2/3 neurons

(A) Schematics of the experiment. Top: mEPSCs were recorded from H1aWT and H1aKO mice at P11 (before eye opening) and during the critical period (P23-32). Bottom: H1aWTs either received daily injections of PBS or MPEP from P14 until P23-32.

(B) Average mEPSC traces.

(C,D) Developmental changes in mEPSC amplitude (C, H1aWT: P11=18.8±0.8 pA, n=21; P23-32=11.2±0.2 pA, n=20; unpaired t-test, ****p<0.0001; H1aKO: P11=16.9±0.9 pA, n=16; P23-32=12.5±0.4 pA, n=15; unpaired t-test, ***p<0.001) and frequency (D, H1aWT:

P11=1.5±0.1 Hz, n=21; P23-32=4.2±0.4 Hz, n=20; unpaired t-test, ****p<0.0001; H1aKO: P11=1.0±0.2 Hz, n=16; P23-32=5.0±0.4 Hz, n=15; unpaired t-test, ****p<0.0001). Average mEPSC amplitude and frequency of H1aWT treated with PBS (orange circle) and MPEP (red triangle) are overlaid on each graph.

Note: For all panels, the datasets for P23-P30 group are a replot of the NR data shown in Figure 3.

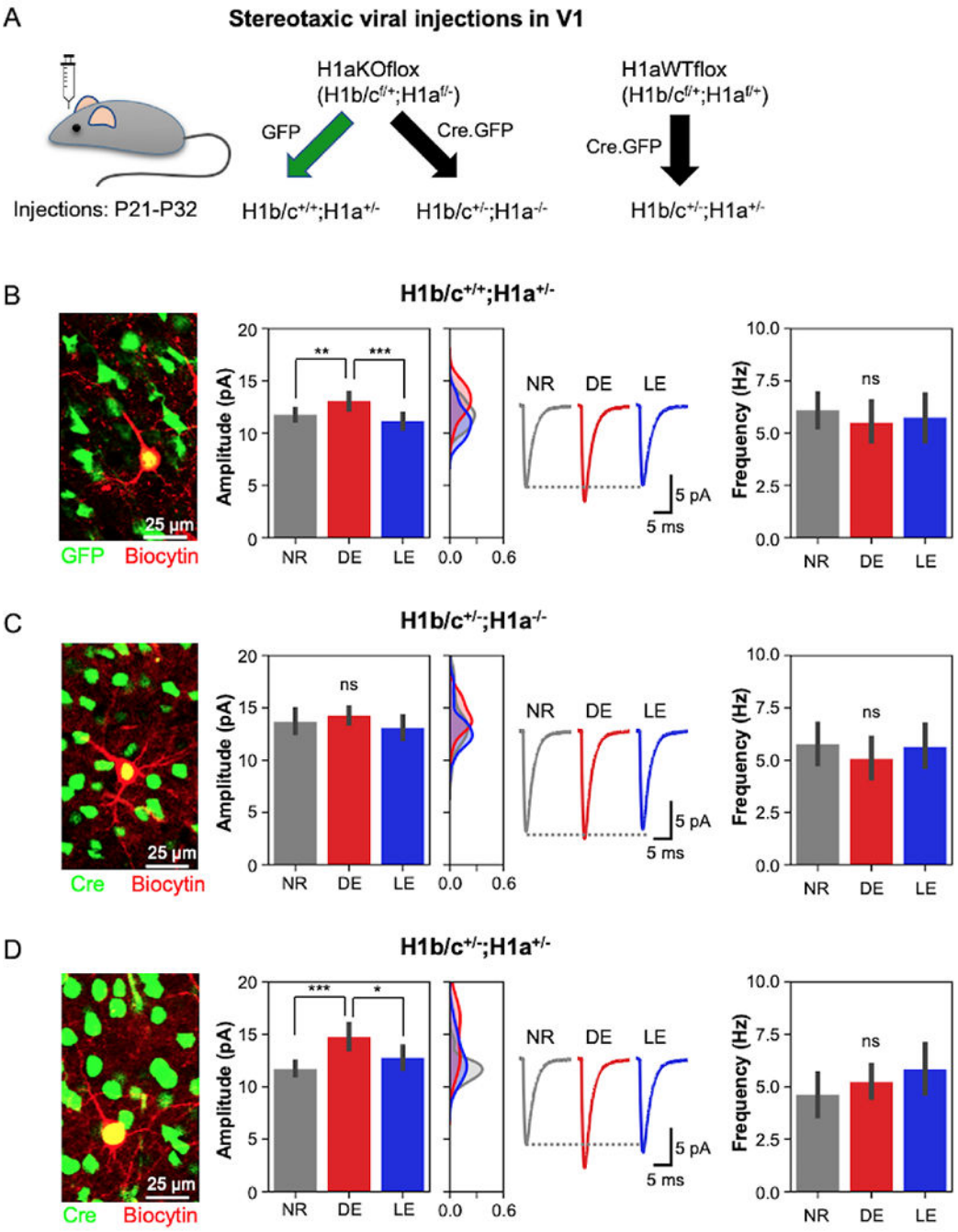

Figure 5. Postnatal H1a expression is required for visual experience-dependent regulation of mEPSCs.

(A) Genotype scheme for producing conditional H1aKO. Survival surgeries were performed to inject AAV containing Cre in mouse V1 L2/3 neurons (age at injection P21-30). To localize H1a primarily in excitatory neurons, Cre expression was driven by CaMKII promoter and GFP was tagged as a reporter for expression. Control mice were injected with only CaMKII-driven GFP. MEPSC recordings were performed in GFP-expressing neurons at P28-45.

(B-D) Lack of visual experience-dependent plasticity of mEPSCs in acute postnatal H1aKO neurons (H1b/c$^{+/-}$;H1a$^{-/-}$). First panel: Confocal image of a recorded neuron (red, filled with biocytin) also expressing Cre-GFP (green). Second panel: Comparison of average amplitude of mEPSCs (B, H1b/c$^{+/+}$;H1a$^{+/-}$: NR=11.8±0.3 pA, n=17; DE=13.1±0.4 pA, n=14; LE=11.1±0.4 pA, n=16; ANOVA, F(2,44)=8.031, p<0.005; C, H1b/c$^{+/-}$;H1a$^{-/-}$: NR=13.7±0.6 pA, n=17; DE=14.3±0.4 pA, n=14; LE=13.1±0.6 pA, n=12; ANOVA, F(2,40)=1.143, p>0.3; D, H1b/c$^{+/-}$;H1a$^{+/-}$: NR=11.7±0.3 pA, n=12; DE=14.7±0.6 pA, n=16; LE=12.8±0.5 pA, n=14; ANOVA, F(2,39)=8.229, p<0.005; Newman-Keuls multiple comparison *p<0.05, **p<0.01, ***p<0.001). Third panel: Estimated population density plot of mEPSC amplitudes (X-axis: Estimated probability density). Fourth panel: Average mEPSC traces. Fifth panel: Comparison of average mEPSC frequency (B, H1b/c$^{+/+}$;H1a$^{+/-}$: NR=6.1±0.4 Hz, n=17; DE=5.5±0.5 Hz, n=14; LE=5.7±0.6 Hz, n=16; ANOVA, F(2,44)=0.3479, p>0.7; C, H1b/c$^{+/-}$;H1a$^{-/-}$: NR=5.8±0.5 Hz, n=17; DE=5.1±0.5 Hz, n=14; LE=5.6±0.5 Hz, n=12; ANOVA, F(2,40)=0.5313, p>0.5; D, H1b/c$^{+/-}$;H1a$^{+/-}$: NR=4.6±0.6 Hz, n=12; DE=5.2±0.4 Hz, n=16; LE=5.8±0.6 Hz, n=14; ANOVA, F(2,39)=1.202, p>0.3). Also see Figure S4 and Table S1.

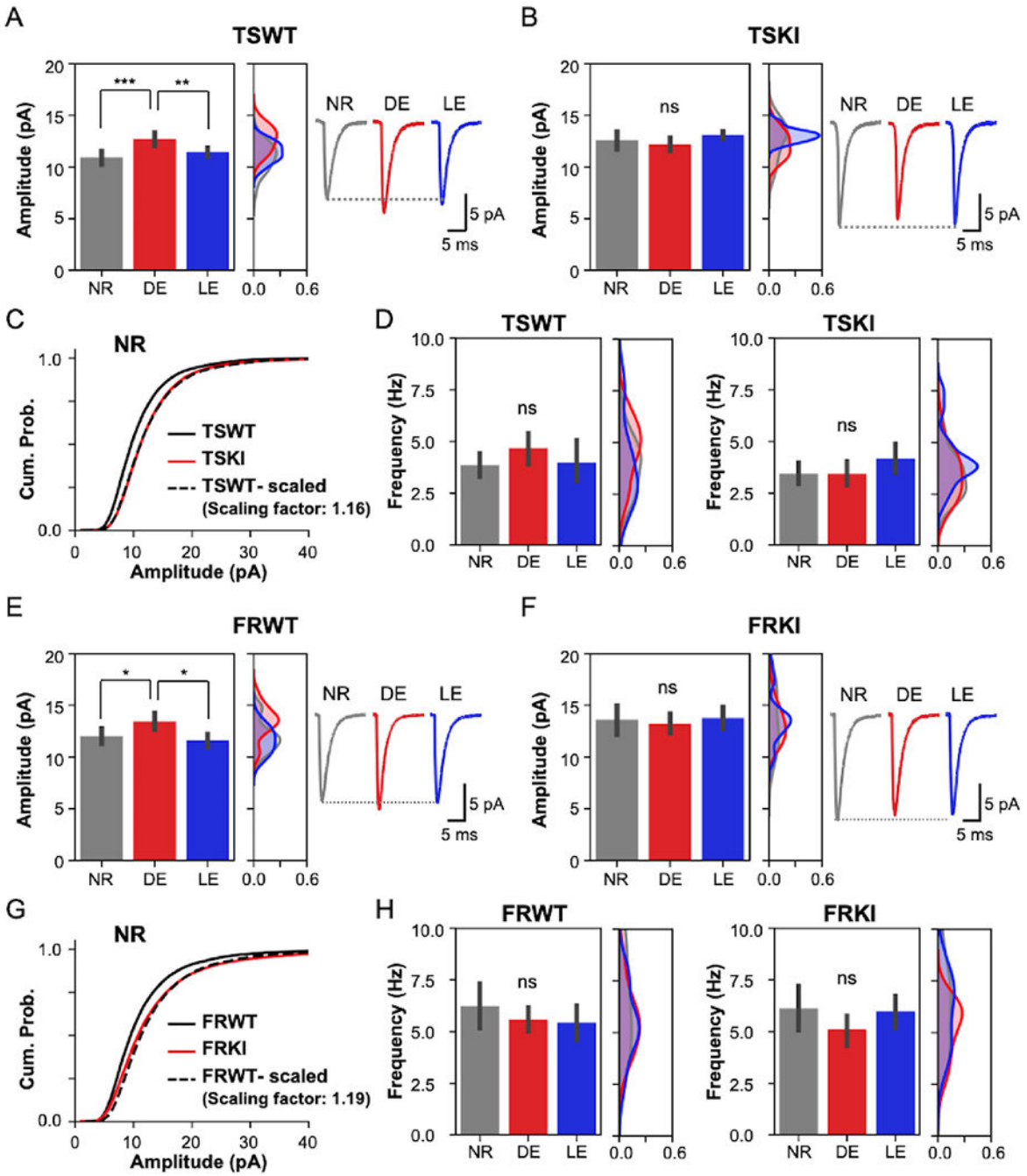

Figure 6. mGluR5-H1a interaction is indispensable for homeostatic decrease in mEPSC amplitude in V1 L2/3 neurons

mEPSC recordings were done in V1 slices from juvenile mice (P23-32).

(A,B) TSKI lack visual experience-dependent homeostatic plasticity. Left: Average mEPSC amplitude comparison (A, TSWT: NR=10.9±0.3 pA, n=18; DE=12.7±0.3 pA, n=12; LE=11.4±0.2 pA, n=16; ANOVA, $F(2,43)=8.295$, $p<0.001$; Newman-Keuls multiple comparison, ***$p<0.001$, **$p<0.01$; B, TSKI: NR=12.6±0.4 pA, n=18; DE=12.2±0.3 pA, n=16; LE=13.1±0.2 pA, n=15; ANOVA, $F(2,46)=1.716$, $p>0.19$). Middle: Estimated population density plot of mEPSC amplitudes (X-axis, Estimated probability density).

Right: Average mEPSC traces. TSKIs showed a significant change in the variance of the estimated population density probability of mEPSC amplitudes (see Table S1).
(C) Cumulative probability of mEPSC amplitudes of NR TSWT (black solid line) overlaid with that of NR TSKI (blue solid line) showing a multiplicative increase. Cumulative probability curve of TSWT mEPSC amplitudes multiplied by a scaling factor (1.16; black dashed line) overlaps with the TSKI curve. Mann-Whitney test: NR-TSWT vs. NR-TSKI, $p<0.0001$; NR-TSWT-scaled vs. NR-TSKI, $p>0.9$. Also see Figure S3.
(D) No change in mEPSC frequency across groups. First panel: Average mEPSC frequency in TSWT (NR=3.8±0.3 Hz, n=18; DE=4.7±0.4 Hz, n=12; LE=4.0±0.5 Hz, n=16; ANOVA, $F(2,43)=0.9937$, $p>0.37$). Second panel: Estimated population density plot of mEPSC frequencies (X-axis: Estimated probability density). Third pane: Average mEPSC frequency in TSKI (NR=3.4±0.3 Hz, n=18; DE=3.4±0.3 Hz, n=16; LE =4.2±0.4 Hz, n=15; ANOVA, $F(2,46)=1.798$, $p>0.17$). Fourth panel: Estimated population density plot (X-axis, Estimated probability density).
(E,F) FRKIs fail to weaken synaptic strength with LE. Left: Comparison of average mEPSC amplitude (E, FRWT: NR=11.5±0.4 pA, n=18; DE=13.0±0.4 pA, n=26; LE=11.8±0.4 pA, n=17; ANOVA, $F(2,58)=4.600$, $p<0.05$; Newman-Keuls multiple comparison $*p < 0.05$; F, FRKI: NR=13.6±0.8 pA, n=14; DE=13.2±0.5 pA, n=12; LE=13.8±0.6 pA, n=17; ANOVA, $F(2,40)=0.1870$, $p>0.8$). Middle: Estimated population density plot (X-axis: Estimated probability density). Right: Average mEPSC traces.
(G) FRKIs display a non-multiplicative increase in basal mEPSC amplitudes compared to FRWT. Mann-Whitney: NR-FRWT (black solid line) vs. NR-FRKI (blue solid line), $p<0.0001$; NR-FRKI vs. NR-FRWT-scaled (black dashed line, scaling factor=1.19), $p<0.0001$.
(H) No change in mEPSC frequency across groups. First panel: Comparison of average mEPSC frequency of FRWTs (NR=6.2±0.6 Hz, n=18; DE=5.6±0.3 Hz, n=26; LE=5.4±0.4 Hz, n=17; ANOVA, $F(2,58)=0.9287$, $p>0.4$). Second panel: Estimated population density plot (X-axis: Estimated probability density). Third pane: Average mEPSC frequency in FRKI (NR=6.1±0.6 Hz, n=14; DE=5.1±0.4 Hz, n=12; LE=6.0±0.4 Hz, n=17; ANOVA, $F(2,40)=1.252$, $p>0.29$). Fourth panel: Estimated population density plot (X-axis: Estimated probability density).
Also see Table S1.

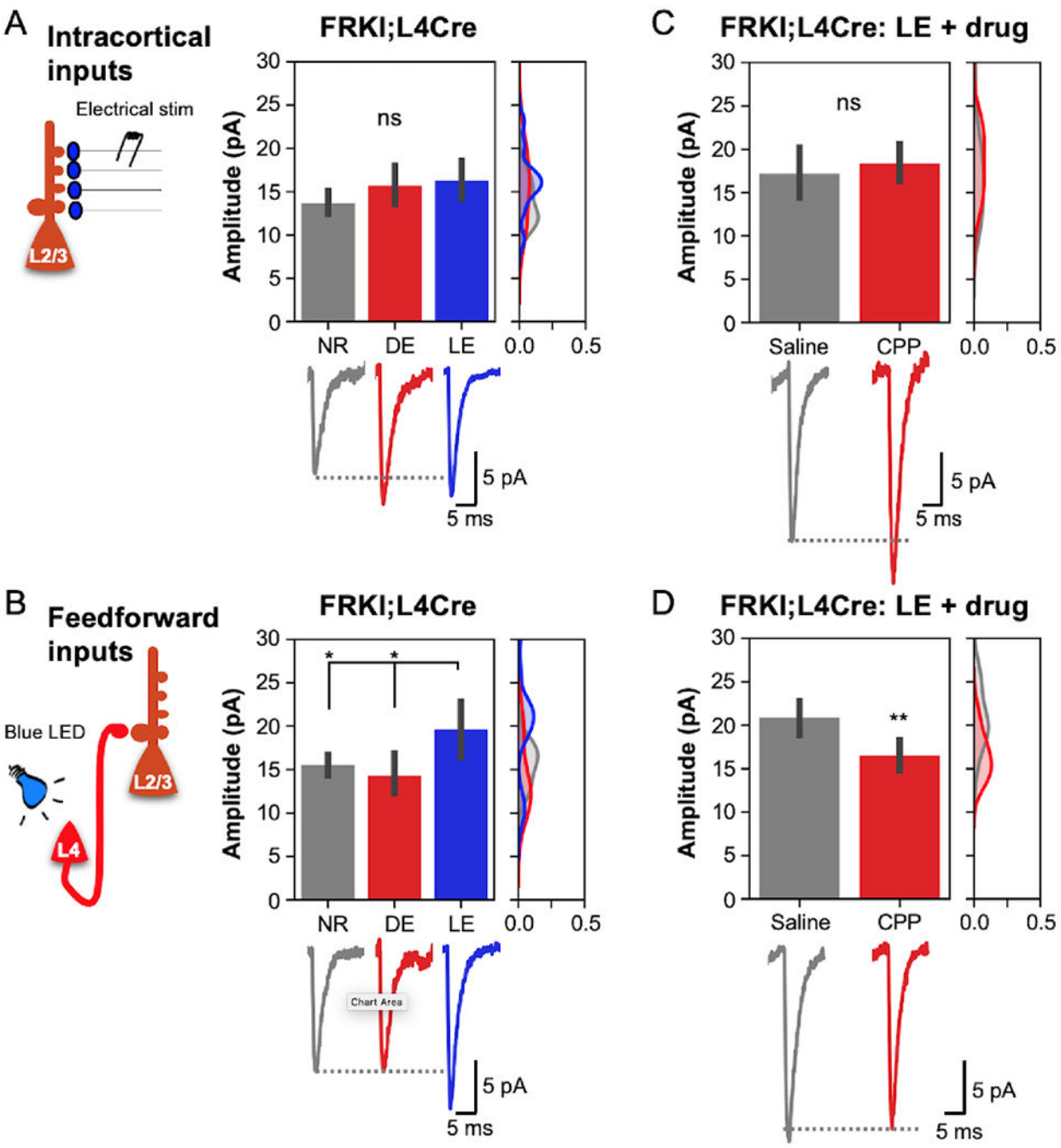

Figure 7. Input-specific depression of IC inputs to L2/3 is dependent on mGluR5-H1a interaction.

(A,B) FRKI;L4Cre mice lack depression of IC inputs, but display aberrant increase in FF inputs, with LE. First panel: Schematics of the experiment. Second panel: Comparison of calculated average evoked Sr^{2+}-mEPSC amplitude measured in L2/3 neurons of FRKI;L4Cre mice (P70-120) (A, IC inputs: NR=13.7±0.8 pA, n=9; DE=15.7±1.2 pA, n=12; LE=16.3±1.2 pA, n=10; ANOVA, $F(2,28)=1.361$, $p>0.27$; B, FF inputs: NR=15.5±0.6 pA, n=12; DE=14.3±1.3 pA, n=10; LE=19.6±1.7 pA, n=13; ANOVA, $F(2,32)=4.647$, $p<0.05$; Newman-Keuls multiple comparison *$p<0.05$). Estimated population density plot (X-axis,

Estimated probability density) is shown next to the bar graphs. Bottom: Average Sr^{2+}-mEPSC traces.

(C,D) NMDAR activity is involved in the aberrant increase of FF input in FRKI;L4Cre mice. Systemic injection of NMDAR antagonist CPP (10 mg/kg, i.p.) 30 min prior to LE does not alter the strength of IC inputs (C, LE+Saline=17.2±1.5 pA, n=12; LE+CPP=18.3±1.2 pA, n=10; unpaired t-test, p=0.560), but prevents the aberrant increase in Sr^{2+}-mEPSC amplitudes for FF inputs (D, LE+Saline =20.9±1.1 pA, n=10; LE+CPP=17.4±0.9 pA, n=10; unpaired t-test, *p=0.026). Estimated population density plots (X-axis: Estimated probability density) are shown next to each bar graph. Bottom: average Sr^{2+}-mEPSC traces.

Also see Table S1.

REAGENT or RESOURCE	SOURCE	IDENTIFIER
Antibodies		
GluA1	Millipore (Rabbit)	Millipore Cat# AB1504; RRID:AB_2113602
GluA2	Millipore (Mouse)	Millipore Cat# MAB397; RRID:AB_2113875
mGluR5	Millipore (Rabbit)	Millipore Cat# AB5675; RRID:AB_2295173
NR1	Huganir lab (JHU, Baltimore) (Rabbit)	N/A
NR2A	Millipore (Rabbit)	Millipore Cat# 07-632; RRID:AB_310837
NR2B	Thermo Fisher Scientific (Rabbit)	Thermo Fisher Scientific Cat# 71-8600; RRID:AB_2534001
Tubulin	Millipore (Mouse)	Millipore Cat# 05-559; RRID:AB_309804
H1b/c	Worley lab (JHU, Baltimore) (Rabbit)	N/A
H1a	Worley lab (JHU, Baltimore) (Rabbit)	N/A (Same as H1b/c)
Goat anti-rabbit Cy5	GE Healthcare	GE Healthcare Cat# PA45011, RRID:AB_772205
Goat anti-mouse Cy3	GE Healthcare	GE Healthcare Cat# PA43010, RRID:AB_772196
Goat anti-mouse Cy5	GE Healthcare	GE Healthcare Cat# PA45010, RRID:AB_772198
Goat anti-rabbit alkaline phosphatase-tagged secondary antibody	Thermo Fisher Scientific	Thermo Fisher Scientific Cat# 31340, RRID:AB_228339
goat anti-mouse Cy3	GE Healthcare	GE Healthcare Cat# PA43010, RRID:AB_772196
Bacterial and Virus Strains		
AAV9.EF1.dflox.hChR2(H134R)-mCherry.WPRE.hGH,	Gift from Karl Diesseroth; Addgene viral prep # 20297-AAV9; http://n2t.net/addgene:20297	Addgene_20297
AAV9.EF1a.DIO.hChR2(H134R).EYFP.WPRE.HGHpA	Gift from Karl Diesseroth; Addgene viral prep # 20298-AAV9; http://n2t.net/addgene:20298	Addgene_20298
AAV9.CamKII.HI.eGFP-Cre.WPRE.SV40	Gift from James M. Wilson; Addgene viral prep # 105551-AAV9; http://n2t.net/addgene:105551	Addgene_105551
AAV9.CamKII0.4.eGFP.WPRE.Rbg	Gift from James M. Wilson; Addgene viral prep # 105541-AAV9; http://n2t.net/addgene:105541	Addgene_105541
Biological Samples		
Chemicals, Peptides, and Recombinant Proteins		
DAPI	Thermo Fisher Scientific	Cat# D-1306; RRID: AB_2629482
Avidin-Texas red conjugate	Life technologies	Cat# A-820

REAGENT or RESOURCE	SOURCE	IDENTIFIER
Formalin	Sigma-Aldrich	Cat# HT5014; MDL: MFCD00003274
Biocytin	Sigma-Aldrich	Cat# B4261
Isoflurane	Patterson Veterinary	Cat# 07-890-8115
Tetrodotoxin citrate (TTX)	Abcam	Cat# ab120055
DL-APV	Sigma-Aldrich	Cat# A5282
glycine	Fisher	Cat# BP381-1
Disodium-ATP	Sigma-Aldrich	Cat# A6419
Disodium-phosphocreatine	Sigma-Aldrich	Cat# P7936
Sodium-GTP	Sigma-Aldrich	Cat# G8877
Lidocaine N-ethyl bromide	Sigma-Aldrich	Cat# L5783
ECF substrate	GE Healthcare	GE Healthcare Cat# RPN5785
Bicuculline methiodide	Enzo	Cat# BML-EA149-0050
MPEP hydrochloride (MPEP)	Tocris	Cat# 1212
Bay36-7620	Tocris	Cat# 2501
AIDA	Tocris	Cat# 0904
(R)-CPPene (CPP)	Abcam	Cat# ab120232
EZ-LinkTM Sulfo NHS-SS-Biotin	Thermo Fisher Scientific	Cat# 21331
Pierce™ NeutrAvidin™ UltraLink™ Resin	Thermo Fisher Scientific	Cat# 53150
Triton X-100	Fisher Scientific	Cat# BP151-100
Prolong Anti-fade mounting media	Invitrogen	Cat# P36930
Trizol-Chloroform RNA extraction reagent	Thermo Fisher Scientific	Cat# 10296-010
RETROscript Reverse Transcription kit	Thermo Fisher Scientific	Cat# AM1710
Maxima SYBR Green/Rox Q-PCR Master mix	Thermo Fisher Scientific	Cat# K0221
Bovine serum albumin	Fisher Scientific	Fisher Scientific Cat#BP1600-1
Critical Commercial Assays		
BCA protein assay kit	Pierce	Cat# 23225
Deposited Data		
Experimental Models: Cell Lines		
Experimental Models: Organisms/Strains		
C57BL/6J	The Jackson Laboratory	RRID: IMSR_JAX:000664
B6;C3-Tg(Scnn1a-cre)3Aibs/J	The Jackson Laboratory	RRID: IMSR_JAX:009613
Floxed-Homer1 (Homer1fl/fl)	Dr. Paul Worley, JHMI	NA
Homer1a knockout (H1aKO)	Dr. Paul Worley, JHMI	NA
mGluR5TS knock in (TSKI)	Dr. Paul Worley, JHMI	NA
mGluR5FR knock in (FRKI)	Dr. Paul Worley, JHMI	NA
Oligonucleotides		
Primer for H1a Forward: CCAGAAAGTATCAATGGGACAGATG	Sigma-Aldrich; {Chiarello, 2013 #61}	N/A

REAGENT or RESOURCE	SOURCE	IDENTIFIER
Primer for H1a Reverse: TGCTGAATTGAATGTGTACCTATGTG	Sigma-Aldrich; {Chiarello, 2013 #61}	N/A
Primer for H1b/c Forward: GGCAAACACTGTTTATGGACTGG	Sigma-Aldrich; {Hu, 2010 #26}	N/A
Primer for H1b/c Reverse: CTCTGTTCTTGGAGTTCTCTGGC	Sigma-Aldrich; {Hu, 2010 #26}	N/A
Primer for GFP Forward: GGTCTTGTAGTTGCCGTGT	Sigma-Aldrich; {Xu, 2012 #62}	N/A
Primer for GFP Reverse: CCTGAAGTTCATCTGCACCA	Sigma-Aldrich; {Xu, 2012 #62}	N/A
Primer for GAPDH Forward: CTGGAGAAACCTGCCAAGTA	Integrated Data Technologies; {Hu, 2010 #26}	N/A
Primer for GAPDH Reverse: AGTGGGAGTTGCTGTTGAAG	Integrated Data Technologies; {Hu, 2010 #26}	N/A
Recombinant DNA		
Software and Algorithms		
Prism 7.0	GraphPad Software	https://www.graphpad.com/scientificsoftware/prism/; RRID: SCR_002798
Igor Pro	Wavemetrics	http://www.wavemetrics.com/products/igorpro/igorpro.htm; RRID:SCR_000325
Mini-Analysis	Synaptosoft	http://www.synaptosoft.com/MiniAnalysis/; RRID:SCR_002184
StepOne Software	Applied Biosystems	RRID:SCR_014281
ImageQuant TL 7.0 software	GE Healthcare	RRID:SCR_014246
Other		
StepOnePlusTM Real-Time PCR system	Applied Biosystems	Cat# 4376600; RRID:SCR_015805
LSM 510 Meta confocal microscope	Zeiss (JHU Integrated imaging center)	RRID:SCR_016187
Spin-X® Acetate Centrifuge Tube filters	Costar	Costar Cat# 8103
Axon patch-clamp amplifier	Molecular Device	Multiclamp 700B
40x Objective lens	Nikon Instruments	Nikon instruments CFI fluor 40X/ 0.80W
Data acquisition board	National instruments	Cat# 779556-01, MDL# BNC-2090A
Digital stimulator	Cygnus Technology Inc.	Cygnus Cat# PG-4000A
Stimulation isolation unit	Cygnus Technology Inc.	Cygnus Cat# SIU91A
0.45 μm pore size PVDF membrane	Biorad	Biorad Cat# 162-0264
Pelco easislicerTM	TedPella	TedPella Cat#11000
0.20 μm pore size Immobilon-P PVDF membrane	Millipore	Millipore Cat# ISEQ00010
Leica microslicer	Leica	Leica Cat#VT1200S